Journal of Computational Acoustics, Vol. 17, No. 3 (2009) 277–308

INTERNATIONAL ASSOCIATION
FOR MATHEMATICS AND
COMPUTERS IN SIMULATION

NEAR-SURFACE LOCALIZATION AND SHAPE IDENTIFICATION OF A SCATTERER EMBEDDED IN A HALFPLANE USING SCALAR WAVES

CHANSEOK JEONG*, SEONG-WON NA† and LOUKAS F. KALLIVOKAS‡

Department of Civil, Architectural and Environmental Engineering
The University of Texas at Austin, Austin, Texas 78712, USA
**chanseok.jeong@gmail.com*
†*swna@mail.utexas.edu*
‡*loukas@mail.utexas.edu*

Received 22 April 2008
Accepted 23 March 2009

We discuss the inverse problem associated with the identification of the location and shape of a scatterer fully embedded in a homogeneous halfplane, using scant surficial measurements of its response to probing scalar waves. The typical applications arise in soils under shear (SH) waves (antiplane motion), or in acoustic fluids under pressure waves. Accordingly, we use measurements of either the Dirichlet-type (displacements), or of the Neumann-type (fluid velocities), to steer the localization and detection processes, targeting rigid and sound-hard objects, respectively. The computational approach for localizing single targets is based on partial-differential-equation-constrained optimization ideas, extending our recent work from the full-[1] to the half-plane case. To improve on the ability of the optimizer to converge to the true shape and location we employ an amplitude-based misfit functional, and embed the inversion process within a frequency- and directionality-continuation scheme, which seem to alleviate solution multiplicity. We use the apparatus of total differentiation to resolve the target's evolving shape during inversion iterations over the shape parameters, à la.[2,3] We report numerical results betraying algorithmic robustness for both the SH and acoustic cases, and for a variety of targets, ranging from circular and elliptical, to potato-, and kite-shaped scatterers.

Keywords: Inverse scattering; shape detection; PDE-constrained optimization; continuation schemes.

1. Introduction

Inverse scattering shape detection problems commonly arise in geophysical probing, in medical ultrasonics, in geotechnical site investigations, and in target identification and acquisition applications. A typical setup consists of an unknown object S embedded within a host medium Ω (Fig. 1).[a] The goal is to locate S and reconstruct its boundary Γ_S, by exploiting the response of the host-object system to incident interrogating waves u^i. The response is

[a]The inverse clutter problem, where multiple objects might be present is not addressed herein.

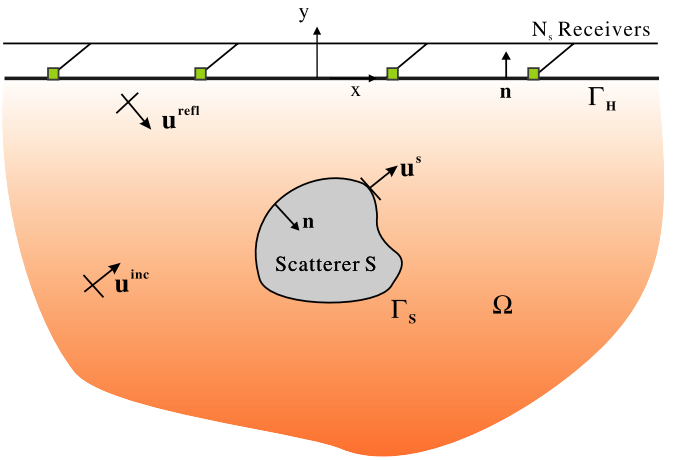

Fig. 1. A model halfplane inverse scattering problem.

typically collected at a few measurement stations or receivers, which, oftentimes, circumscribe the obstacle, either in the near-, or the far-field. For example, in medical imaging applications, it is common that multiple receivers and sources, situated in the near-field, fully surround the probed target, whereas, by contrast, in underwater acoustics, it is the far-field response that drives the detection process, whether sampled at sparsely and irregularly spaced stations (limited aperture), or at stations loosely circumscribing the scatterer.

There is a plethora of approaches and a rich literature devoted to such inverse scattering problems, marked by significant advances over the last 20 years, including classic works by Colton, Kress, Colton *et al.*, and Kirsch.[4–6] However, solution approaches to problems of practical interest aimed at the detection of multiple, deformable, and potentially moving obstacles, embedded within arbitrarily heterogeneous hosts, and, ideally, directly in the time-domain, remain elusive, owing to the yet insurmountable complexity of the underlying mathematical and computational problem. Despite notable exceptions with, for example, background heterogeneity,[7,8] it is, thus, for good reason that most published work in inverse scattering focuses on homogeneous hosts, where gradient-based optimization approaches often serve as the starting point. Typically, misfit functionals describing the difference between measured responses, and those computed owing to an estimate of the shape and location, are sought to be minimized. The process is onerous, and plagued by the usual difficulties associated with inverse problems, namely, solution existence, multiplicity, and ill-conditioning of the numerical processes, in addition to sensitivity with respect to initial estimates of shape and location.

To improve on such algorithms, concurrent linear sampling methods, pioneered by Colton and Kirsch,[9] aim at offering an initial estimate close to the target, thus accelerating global optimization approaches. This is accomplished by essentially sampling the entire domain where the scatterer may lie, via an appropriately constructed probing functional. Closely related approaches, rooted in the topological derivative concept,[10,11] offer improved

capabilities, in that they not only allow preliminary estimates of the geometry, but also of the material composition of the obstacle. The approach has been successfully used in infinite domains involving elastic targets, with recently reported extensions to the semi-infinite case.[12]

In this work, we follow an optimization-based approach, cast within the general framework of partial-differential-equation (PDE)-constrained optimization,[13] using integral equations and boundary elements to resolve the ensuing numerical problem. In principle, the approach also stands to benefit from application of linear sampling or topological derivative concepts, though these are not addressed herein. Much of the foundation for this work has been set by Bonnet,[3] where an elegant framework for tackling such problems using an adjoint formulation and integral equations in the frequency-domain has been discussed, with applications in three dimensions. Here, of particular interest is the easier, yet untackled, two-dimensional problem arising in a semi-infinite medium (Fig. 1), where Ω denotes the negative halfplane, the receivers are all located on the top surface Γ_H (Fig. 1), and the interrogating waves originate from a subsurface disturbance. For this problem, cast in the frequency-domain, we provide the framework based on PDE-constrained optimization ideas, which yield state, adjoint, and control problems — the latter formulated for the first time. We also attempt to improve on the optimizer's chances to converge by implementing three schemes: (a) an amplitude-based misfit functional that presents a less oscillatory profile to the optimizer than typical misfits; (b) a frequency and/or directionality-continuation scheme within which we embed the inversion process; and (c) a stepped approach to location/shape refinement, where the shape of the initial guess remains constrained until the target's location is approached, at which time, the shape-constraint is released to allow shape refinement. In this context, we discuss two different, yet closely related scalar wave cases, namely, the antiplane shear (SH) wave, and the acoustic case, extending our earlier work from the full-[1] to the halfplane case. We consider both Dirichlet-type measurements (e.g. displacements in the SH case) and Neumann-type data (e.g. particle velocities in the acoustic case) in order to construct a misfit functional. The case of Neumann data is onerous for the adjoint problem, and is seldom addressed.

2. Preliminaries

We are concerned with both the SH and the acoustic wave cases, which arise in a homogeneous semi-infinite host, occupied by a linear elastic solid, and an (incompressible) acoustic fluid, respectively. In both cases the wave motions are governed, in the frequency-domain, by Helmholtz equation, with different free surface conditions for each case; the details follow:

2.1. *SH case*

We consider first an immovable rigid obstacle fully buried within a linear elastic homogeneous solid (could be soil) characterized by wave velocity c, and illuminated by an SH incident wave. The scattered motion is governed by the following time-harmonic boundary

value problem[b]:

$$\Delta u^s_{\rm SH}(\mathbf{x}) + k^2 u^s_{\rm SH}(\mathbf{x}) = 0, \quad \mathbf{x} \in \Omega, \tag{1}$$

$$u^t_{\rm SH}(\mathbf{x}) = u^s_{\rm SH}(\mathbf{x}) + u^i(\mathbf{x}) + u^r_{\rm SH}(\mathbf{x}) = 0, \quad \mathbf{x} \in \Gamma_S, \tag{2}$$

$$\frac{\partial u^t_{\rm SH}(\mathbf{x})}{\partial n} = \frac{\partial u^s_{\rm SH}(\mathbf{x})}{\partial n} + \frac{\partial u^i(\mathbf{x})}{\partial n} + \frac{\partial u^r_{\rm SH}(\mathbf{x})}{\partial n} = 0, \quad \mathbf{x} \in \Gamma_H, \tag{3}$$

$$\lim_{r\to\infty} \sqrt{r}\left(\frac{\partial u^s_{\rm SH}}{\partial r} - iku^s_{\rm SH}\right) = 0. \tag{4}$$

Here, $u^s_{\rm SH}$ denotes the antiplane scattered displacement field[c]; $u^t_{\rm SH}$ denotes the total field; $u^r_{\rm SH}$ denotes the free-field reflected wave, that is, the field generated when u^i impinges upon the surface Γ_H in the absence of any scatterer; $\mathbf{x}$ is a position vector; $\mathbf{n}$ is the outward unit normal on Γ_S and Γ_H; Δ is the Laplace operator; k is the wavenumber (i.e. $k = \omega/c$); (2) is the boundary condition on the surface of the scatterer; (3) describes the traction-free boundary condition on Γ_H; and condition (4) is the Sommerfeld radiation condition where r denotes radial distance.

The incident interrogating wavefield u^i describing incoming plane waves, and the free-field reflected wave $u^r_{\rm SH}$ can be expressed as[d]:

$$u^i(x, y, t) = e^{ik(x\cos\alpha + y\sin\alpha)}, \tag{5}$$

$$u^r_{\rm SH}(x, y, t) = e^{ik(x\cos\alpha - y\sin\alpha)}, \tag{6}$$

where α denotes the incidence angle, that is, the angle formed between the x-axis and the normal to the wave propagation front. Notice that, with the definitions (5) and (6), there holds on the traction-free surface Γ_H:

$$\frac{\partial u^i}{\partial n} + \frac{\partial u^r_{\rm SH}}{\partial n} = 0, \quad \text{on } \Gamma_H, \tag{7}$$

which, by virtue of (3) also implies that:

$$\frac{\partial u^s_{\rm SH}}{\partial n} = 0, \quad \text{on } \Gamma_H. \tag{8}$$

We remark that $u^s_{\rm SH}$ does not vanish on the free surface Γ_H; thus, in the SH case, we measure and use the scattered field $u^s_{\rm SH}$ on Γ_H (Dirichlet data) to drive the detection process.

2.2. *Acoustic case*

We now consider Ω to be occupied by an acoustic fluid characterized by a wave velocity c; let S denote a sound-hard scatterer. Then the associated boundary value problem can be

[b]Subscripts SH and AC are used to denote SH and acoustic case fields, respectively.
[c]We remark that $u^s_{\rm SH}$ is only a part of the total scattered field; to obtain the total scattered field, $u^r_{\rm SH}$ needs to be added to $u^s_{\rm SH}$.
[d]Throughout, we assume a common harmonic factor of $e^{-i\omega t}$.

similarly cast as:

$$\Delta u^s_{\rm AC}(\mathbf{x}) + k^2 u^s_{\rm AC}(\mathbf{x}) = 0, \quad \mathbf{x} \in \Omega, \tag{9}$$

$$\frac{\partial u^t_{\rm AC}(\mathbf{x})}{\partial n} = \frac{\partial u^s_{\rm AC}(\mathbf{x})}{\partial n} + \frac{\partial u^i(\mathbf{x})}{\partial n} + \frac{\partial u^r_{\rm AC}(\mathbf{x})}{\partial n} = 0, \quad \mathbf{x} \in \Gamma_S, \tag{10}$$

$$u^t_{\rm AC}(\mathbf{x}) = u^s_{\rm AC}(\mathbf{x}) + u^i(\mathbf{x}) + u^r_{\rm AC}(\mathbf{x}) = 0, \quad \mathbf{x} \in \Gamma_H, \tag{11}$$

$$\lim_{r\to\infty} \sqrt{r}\left(\frac{\partial u^s_{\rm AC}}{\partial r} - iku^s_{\rm AC}\right) = 0, \tag{12}$$

where (11) is the boundary condition on the pressure-free surface. We remark that, whereas the incident pressure field u^i is still given by (5), the free-field reflected field is now expressed by:

$$u^r_{\rm AC}(x, y, t) = -e^{ik(x\cos\alpha - y\sin\alpha)}. \tag{13}$$

Similarly, the following conditions, counterpart to (7) and (8), hold:

$$u^i + u^r_{\rm AC} = 0, \quad \text{on } \Gamma_H, \tag{14}$$

$$u^s_{\rm AC} = 0, \quad \text{on } \Gamma_H. \tag{15}$$

In the acoustic case, we use pressure gradients (or equivalently particle velocities), that is, Neumann data $\partial u^s_{\rm AC}/\partial n$ on the free surface, to drive the inversion.

3. The Forward Problems

We discuss next standard representations to the solution of the forward problems. We favor integral equations and boundary elements, owing, on one hand, to the homogeneity of the background host and, on the other, to the benefit of the *a priori* satisfaction of the radiation condition, and the dimensionality reduction they offer. Specifically, see the following cases.

3.1. *SH case*

The solution to the forward problem in the SH case (1)–(4) is given by the following integral representation:

$$u^t_{\rm SH} = \mathfrak{D}_{\rm SH}[u^t_{\rm SH}] - \mathfrak{S}_{\rm SH}\left[\frac{\partial u^t_{\rm SH}}{\partial n}\right] + u^i + u^r_{\rm SH}, \tag{16}$$

where $\mathfrak{S}_{\rm SH}$ and $\mathfrak{D}_{\rm SH}$ are the single- and double-layers defined for any smooth function f, as[e]:

$$\mathfrak{S}_{\rm SH}[f](\mathbf{x}) = \int_{\Gamma_S} f(\mathbf{y}) G^H_{\rm SH}(\mathbf{x}, \mathbf{y}) {\rm d}\Gamma(\mathbf{y}), \quad \mathbf{x} \in \Omega, \quad \mathbf{y} \in \Gamma_S, \tag{17}$$

$$\mathfrak{D}_{\rm SH}[f](\mathbf{x}) = \int_{\Gamma_S} f(\mathbf{y}) \frac{\partial G^H_{\rm SH}(\mathbf{x}, \mathbf{y})}{\partial n_{\mathbf{y}}} {\rm d}\Gamma(\mathbf{y}), \quad \mathbf{x} \in \Omega, \quad \mathbf{y} \in \Gamma_S. \tag{18}$$

[e]Euler script letters (e.g. $\mathfrak{D}_{\rm SH}$) are used to represent the domain layers, i.e. when $\mathbf{x} \in \Omega$, and roman letters (e.g. $D_{\rm SH}$) are used to indicate their boundary counterparts, i.e. when $\mathbf{x} \in \Gamma$.

In the above, the halfplane Green's function $G^H_{\rm SH}$ for the SH case is given by:

$$G^H_{\rm SH}(\mathbf{x},\mathbf{y}) = G(\mathbf{x},\mathbf{y}) + G(\hat{\mathbf{x}},\mathbf{y}) = -\frac{i}{4}(H_0^{(1)}(kr) + H_0^{(1)}(k\hat{r})), \tag{19}$$

where, $r = |\mathbf{x}-\mathbf{y}|$, and $\hat{r} = |\hat{\mathbf{x}}-\mathbf{y}|$; $\hat{\mathbf{x}}$ denotes the mirror point of $\mathbf{x}$ with respect to the free surface ($\hat{\mathbf{x}}$ lies in the positive halfplane); i is the imaginary unit; $H_0^{(1)}(\cdot)$ is the zeroth order Hankel function of the first kind, and G denotes the fullplane Green's function. Moreover, the following jump conditions hold:

$$\lim_{\Omega\ni\mathbf{x}\to\mathbf{x}\in\Gamma_S} \mathfrak{S}_{\rm SH}[f](\mathbf{x}) = S_{\rm SH}[f](\mathbf{x}), \quad \text{or} \quad \mathfrak{S}_{\rm SH}[f] = S_{\rm SH}[f], \tag{20}$$

$$\lim_{\Omega\ni\mathbf{x}\to\mathbf{x}\in\Gamma_S} \mathfrak{D}_{\rm SH}[f](\mathbf{x}) = \frac{1}{2}f(\mathbf{x}) + D_{\rm SH}[f](\mathbf{x}), \quad \text{or} \quad \mathfrak{D}_{\rm SH}[f] = \frac{1}{2}f + D_{\rm SH}[f], \tag{21}$$

where,

$$S_{\rm SH}[f](\mathbf{x}) = \int_{\Gamma_S} f(\mathbf{y}) G^H_{\rm SH}(\mathbf{x},\mathbf{y}) \mathrm{d}\Gamma(\mathbf{y}), \quad \mathbf{x},\mathbf{y}\in\Gamma_S, \tag{22}$$

$$D_{\rm SH}[f](\mathbf{x}) = \int_{\Gamma_S} f(\mathbf{y}) \frac{\partial G^H_{\rm SH}(\mathbf{x},\mathbf{y})}{\partial n_{\mathbf{y}}} \mathrm{d}\Gamma(\mathbf{y}), \quad \mathbf{x},\mathbf{y}\in\Gamma_S. \tag{23}$$

As a result of the jump conditions and the boundary condition (2) on Γ_S, i.e. that $u^t_{\rm SH} = 0$, (16) reduces to:

$$S_{\rm SH}\left[\frac{\partial u^t_{\rm SH}}{\partial n}\right] = u^i + u^r_{\rm SH}, \quad \text{on } \Gamma_S. \tag{24}$$

Boundary integral equation (24) can be used in solving the forward problem in the SH case.

3.2. *Acoustic case*

Similarly, the forward problem in the acoustic case, described by (9)–(12), can be solved by using the following integral equation:

$$u^t_{\rm AC} = \mathfrak{D}_{\rm AC}[u^t_{\rm AC}] - \mathfrak{S}_{\rm AC}\left[\frac{\partial u^t_{\rm AC}}{\partial n}\right] + u^i + u^r_{\rm AC}, \tag{25}$$

where,

$$\mathfrak{S}_{\rm AC}[f](\mathbf{x}) = \int_{\Gamma_S} f(\mathbf{y}) G^H_{\rm AC}(\mathbf{x},\mathbf{y}) \mathrm{d}\Gamma_S(\mathbf{y}), \quad \mathbf{x}\in\Omega, \mathbf{y}\in\Gamma_S, \tag{26}$$

$$\mathfrak{D}_{\rm AC}[f](\mathbf{x}) = \int_{\Gamma_S} f(\mathbf{y}) \frac{\partial G^H_{\rm AC}(\mathbf{x},\mathbf{y})}{\partial n_{\mathbf{y}}} \mathrm{d}\Gamma_S(\mathbf{y}), \quad \mathbf{x}\in\Omega, \mathbf{y}\in\Gamma_S. \tag{27}$$

In the acoustic case, the halfplane Green's function is given by:

$$G^H_{\rm AC}(\mathbf{x},\mathbf{y}) = G(\mathbf{x},\mathbf{y}) - G(\hat{\mathbf{x}},\mathbf{y}) = -\frac{i}{4}(H_0^{(1)}(kr) - H_0^{(1)}(k\hat{r})). \tag{28}$$

By virtue again of the jump conditions (20) and (21), and the Neumann condition (10), (25) reduces to

$$\frac{1}{2}u^t_{\mathrm{AC}} - D_{\mathrm{AC}}[u^t_{\mathrm{AC}}] = u^i + u^r_{\mathrm{AC}}, \quad \text{on } \Gamma_S. \tag{29}$$

Boundary integral equation (29) is used for the solution of the forward problem in the acoustic case.

4. The Inverse Problems

We are interested in localizing Γ_S, while also reconstructing its shape, using surficial measurements that correspond to the response of the host and obstacle system to an illuminating wave. For both the SH and acoustic cases, we use the apparatus of PDE-constrained optimization. To this end, we first construct a misfit functional between measured and computed data, and then augment it via the weak imposition of the governing PDEs, to arrive at an unconstrained minimization problem amenable to classical optimization techniques. Below, we sketch the technical details; we again distinguish two cases.

4.1. *Misfit functional choice*

Classical lines in full waveform inversion problems, suggest the construction of a misfit functional as a starting point. Here, we considered two possible choices for the misfit functional, both normalized with respect to the amplitudes of the measured response:

$$\mathcal{L}(u^s) = \frac{1}{2}\sum_{j=1}^{N_s} \frac{\{|u^s(\mathbf{x}_j,\xi)| - |u^s_m(\mathbf{x}_j)|\}^2}{|u^s_m(\mathbf{x}_j)|^2}, \tag{30}$$

$$\mathcal{L}_c(u^s) = \frac{1}{2}\sum_{j=1}^{N_s} \frac{|u^s(\mathbf{x}_j,\xi) - u^s_m(\mathbf{x}_j)|^2}{|u^s_m(\mathbf{x}_j)|^2}. \tag{31}$$

In the above $u^s(\mathbf{x}_j,\xi)$ denotes computed response (complex), and $u^s_m(\mathbf{x}_j)$ denotes measured response (also complex), both evaluated at the jth station/receiver location. Misfit (30) represents the real-valued difference between measured and computed amplitudes, whereas misfit (31) is the amplitude of the difference between the complex-valued computed and measured responses. Notice that, whereas the functional in (31) clearly accounts for both amplitude and phase, the phase information is not entirely lost in the amplitude-based functional (30). The misfit (31) is a typical choice in full waveform inversion; here, however, we opt for the amplitude-based misfit (30). To illustrate the rationale for this choice we review next a simple problem, schematically depicted in Fig. 2.

We first measure (compute) the response of the depicted system at the receiver locations situated at $(-7,0),(0,0)$, and $(7,0)$, for an incoming plane wave (at three different frequencies), and for the true location of a circular scatterer of unit radius whose center coordinates (x_0,y_0) are $(0,-10)$. Then we vary the center coordinates of a guessed circular scatterer of

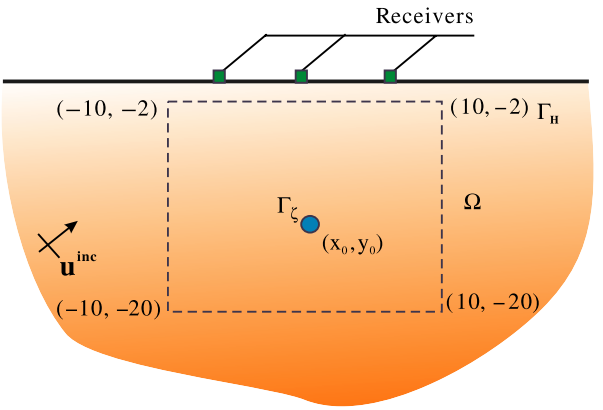

Fig. 2. A scattering problem to highlight misfit functional preference. The misfits are computed for varying positions of a unit radius circular scatterer within the dotted rectangle; the true target is located at $(0, -10)$. The receivers are placed at $(-7, 0)$, $(0, 0)$, $(7, 0)$.

a unit radius within the dotted rectangle shown in Fig. 2: for each scatterer location, we record the misfits computed using both (30) and (31). Figure 3 depicts the variation of the misfits for the possible scatterer locations. Therein, it appears that the amplitude-based misfit functional (30) appears less oscillatory than misfit (31). Based on this observation and on prior experience with similar problems in the fullplane case,[1] we favor the use of the amplitude-based misfit (30).

4.2. *SH case*

With the choice of (30), seeking the location and the shape of the scatterer is tantamount to a governing PDE-constrained minimization problem, whereby one tries to minimize the misfit subject to the physics of the problem, as the latter are described by the governing

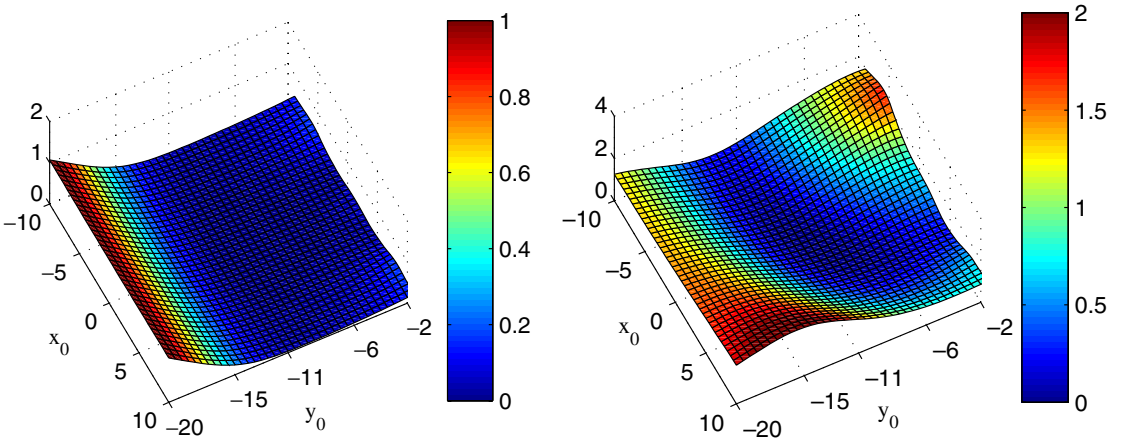

(a) $k = 0.1$, Amplitude-based $\mathcal{L}$ (b) $k = 0.1$, Misfit $\mathcal{L}_c$

Fig. 3. Misfit behavior as a function of the scatterer's location.

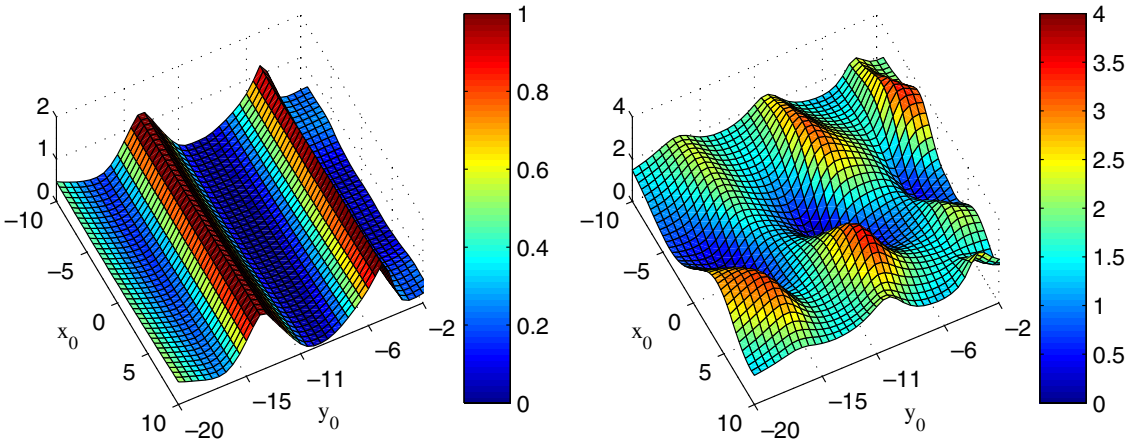

(c) $k = 0.5$, Amplitude-based $\mathcal{L}$ (d) $k = 0.5$, Misfit $\mathcal{L}_c$

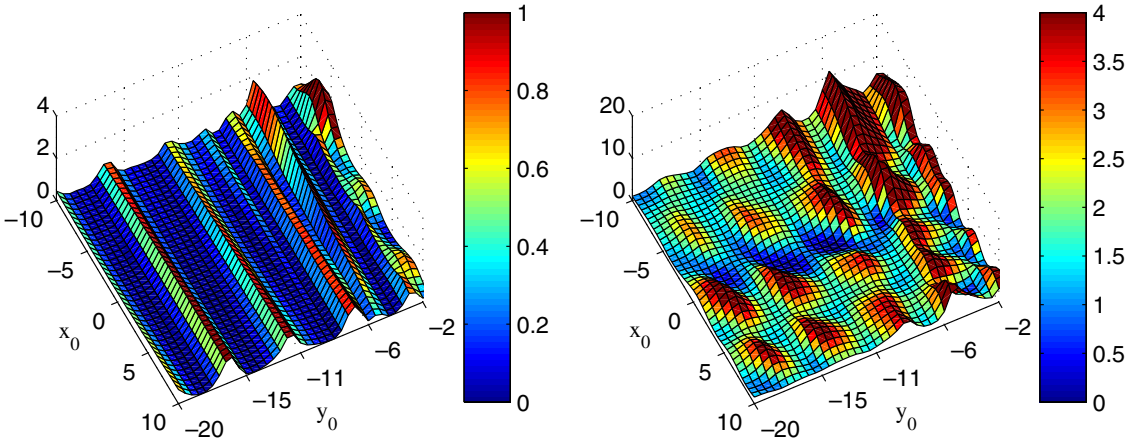

(e) $k = 1.0$, Amplitude-based $\mathcal{L}$ (f) $k = 1.0$, Misfit $\mathcal{L}_c$

Fig. 3. (*Continued*)

PDEs. A key step of the methodology followed herein is the casting of the constrained optimization problem as an unconstrained one via the weak imposition of the PDEs. To this end, we construct next an augmented functional — augmented via the side imposition of the forward problem, (1)–(4). There results:

$$\begin{aligned}\mathcal{A}_{\mathrm{SH}}(u^s_{\mathrm{SH}},\lambda,\xi) = \frac{1}{2}\sum_{j=1}^{N_s}\frac{\{|u^s_{\mathrm{SH}}(\mathbf{x}_j,\xi)| - |u^s_m(\mathbf{x}_j)|\}^2}{|u^s_m(\mathbf{x}_j)|^2}\\ + \Re e\left\{\int_{\Omega^\xi}\lambda(\mathbf{x}^\xi,\xi)[\Delta u^s_{\mathrm{SH}}(\mathbf{x}^\xi,\xi) + k^2 u^s_{\mathrm{SH}}(\mathbf{x}^\xi,\xi)]\mathrm{d}\Omega^\xi\right.\\ \left. - \int_{\Gamma^\xi}\lambda_D(\mathbf{x}^\xi,\xi)[u^s_{\mathrm{SH}}(\mathbf{x}^\xi,\xi) + u^i(\mathbf{x}^\xi) + u^r_{\mathrm{SH}}(\mathbf{x}^\xi)]\mathrm{d}\Gamma^\xi\right.\end{aligned}$$

$$- \int_{\Gamma_H} \lambda(\mathbf{x}^\xi, \xi) \left[\frac{\partial u^s_{\mathrm{SH}}}{\partial n}(\mathbf{x}^\xi, \xi) + \frac{\partial u^i}{\partial n}(\mathbf{x}^\xi) + \frac{\partial u^r_{\mathrm{SH}}}{\partial n}(\mathbf{x}^\xi) \right] \mathrm{d}\Gamma_H$$

$$- \int_{\Gamma_\infty} \lambda(\mathbf{x}^\xi, \xi) \left[\frac{\partial u^s_{\mathrm{SH}}}{\partial r}(\mathbf{x}^\xi, \xi) - iku^s_{\mathrm{SH}}(\mathbf{x}^\xi, \xi) \right] \mathrm{d}\Gamma_\infty \Bigg\}. \tag{32}$$

In (32), λ denotes Lagrange multiplier; λ_D also denotes a Lagrange multiplier used to enforce weakly the essential boundary condition (2) (λ and λ_D have different physical dimensions). Notice that only the real part of the weak imposition of the strong form appears in (32), since this is sufficient for ensuring that the strong form is satisfied, while conveniently allowing for a real-valued functional, which greatly facilitates the associated numerical process. Notice further that, in (32), various quantities depend on the scalar parameter ξ: during the search for the optimum of $\mathcal{A}_{\mathrm{SH}}$, the location and boundary description of the scatterer changes, that is, the boundary evolves and the parameter ξ is used as a metric to describe the scatterer's boundary evolution during the search iterations. In particular, in the above Γ^ξ represents one possible instantiation of Γ_S. Furthermore, since, when the boundary Γ^ξ changes, the surrounding domain changes as well, and thus Ω too depends on ξ; we use Ω^ξ to denote this dependence.

4.2.1. *Evolving boundary shape treatment*

To describe shape evolution between successive updates of the boundary parameterization during the search for the target, we adopt the concept of a moving boundary.[2,3] We assume that the boundary evolution is driven by a transformational velocity field $\mathbf{v}$ (Fig. 4). In general, this velocity field can be described in terms of two components, one along the normal and one along the tangential to the boundary directions. We shall henceforth assume that the boundary evolves due only to the normal velocity component v_n; for small shape perturbations, this is a nonrestrictive assumption.[14] Let $\mathbf{x}$ be a point on the boundary Γ (Fig. 4).[f] Then, driven by the velocity v_n, Γ evolves to Γ^ξ, and $\mathbf{x}$ becomes such that:

$$\Gamma \ni \mathbf{x} \to \mathbf{x} + \xi v_n(\mathbf{x})\mathbf{n}(\mathbf{x}) \equiv \mathbf{x}^\xi \in \Gamma^\xi, \tag{33}$$

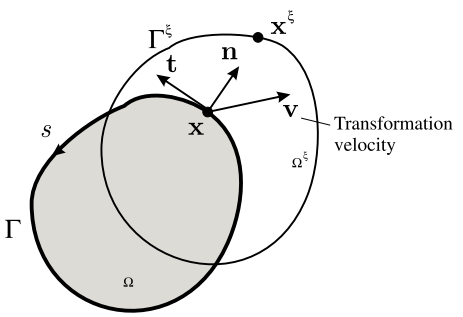

Fig. 4. Boundary shape evolution under a transformational velocity field.

[f]Here, we treat Γ as the boundary corresponding to the previous iteration; upon convergence, $\Gamma \equiv \Gamma_S$.

where $\mathbf{n}$ is the normal to the boundary, and, when v_n is known, the scalar parameter ξ is all that is needed to characterize the evolving shape.

In establishing the first-order optimality conditions associated with the augmented functional (32), there is a need to express the derivatives of a scalar function, and of line and domain integrals defined over Γ^ξ and Ω^ξ, with respect to ξ (such derivatives are referred to in the literature as total, or Eulerian, or material, or shape derivatives). Accordingly, let $f(\mathbf{x}^\xi, \xi)$ denote a scalar function defined over Ω^ξ. Then[14]:

$$\left[\frac{Df(\mathbf{x}^\xi,\xi)}{D\xi}\right]_{\xi=0} = \left[\dot{f} + v_n \frac{\partial f}{\partial n}\right], \tag{34}$$

$$\left[\frac{D}{D\xi}\int_{\Gamma^\xi} f(\mathbf{x}^\xi,\xi)\mathrm{d}\Gamma^\xi\right]_{\xi=0} = \int_\Gamma \left[\dot{f} + v_n\frac{\partial f}{\partial n} - \kappa f v_n\right]\mathrm{d}\Gamma, \tag{35}$$

$$\left[\frac{D}{D\xi}\int_{\Omega^\xi} f(\mathbf{x}^\xi,\xi)\mathrm{d}\Omega^\xi\right]_{\xi=0} = \int_\Omega \dot{f}\mathrm{d}\Omega + \int_\Gamma f v_n \mathrm{d}\Gamma, \tag{36}$$

where $\dot{f} = \partial f/\partial\xi$; $D/D\xi$ denotes total derivative; and κ denotes the curvature of the boundary Γ.

4.2.2. *The first-order optimality conditions*

To arrive at the first-order optimality conditions, we require that variations of the augmented functional $\mathcal{A}_{\mathrm{SH}}$ with respect to the Lagrange multipliers λ (henceforth referred to as the adjoint variables), the state variable u^s_{SH}, and the boundary metric ξ,[1] vanish. We remark that the variation with respect to ξ above is equivalent to the variation with respect to the shape perturbation parameters that represent the control variables in this inverse problem. Accordingly:

$$\left\{\begin{array}{c} \delta_\lambda \mathcal{A}_{\mathrm{SH}} \\ \delta_{\lambda_D}\mathcal{A}_{\mathrm{SH}} \\ \delta_{u^s_{\mathrm{SH}}}\mathcal{A}_{\mathrm{SH}} \\ \delta_\xi \mathcal{A}_{\mathrm{SH}} \end{array}\right\} = \mathbf{0}. \tag{37}$$

Upon discretization, (37) will lead to a classic Karush–Kuhn–Tucker (KKT) system.[15,16] Next, we expand (37); variations of $\mathcal{A}_{\mathrm{SH}}$ with respect to the adjoint variables λ and λ_D, yield:

$$\delta_\lambda \mathcal{A}_{\mathrm{SH}} = \Re e\Bigg\{\int_{\Omega^\xi}\delta\lambda(\Delta u^s_{\mathrm{SH}} + k^2 u^s_{\mathrm{SH}})\mathrm{d}\Omega^\xi - \int_{\Gamma_H}\delta\lambda\left(\frac{\partial u^s_{\mathrm{SH}}}{\partial n} + \frac{\partial u^i}{\partial n} + \frac{\partial u^r_{\mathrm{SH}}}{\partial n}\right)\mathrm{d}\Gamma_H$$
$$- \int_{\Gamma_\infty}\delta\lambda\left(\frac{\partial u^s_{\mathrm{SH}}}{\partial r} - iku^s_{\mathrm{SH}}\right)\mathrm{d}\Gamma_\infty\Bigg\} = 0, \tag{38}$$

$$\delta_{\lambda_D}\mathcal{A}_{\mathrm{SH}} = \Re e\Bigg\{-\int_{\Gamma^\xi}\delta\lambda_D(u^s_{\mathrm{SH}} + u^i + u^r_{\mathrm{SH}})\mathrm{d}\Gamma^\xi\Bigg\} = 0. \tag{39}$$

Clearly, for arbitrary $\delta\lambda$ and $\delta\lambda_D$, the vanishing of the variations in (38) and (39) recovers the forward (or state) problem (1)–(4) for any instantiation of Γ^ξ and Ω^ξ. Accordingly:

State problem:

$$\begin{aligned}
\Delta u^s_{\rm SH}(\mathbf{x}) + k^2 u^s_{\rm SH}(\mathbf{x}) = 0, \quad & \mathbf{x} \in \Omega^\xi, \\
u^s_{\rm SH}(\mathbf{x}) + u^i(\mathbf{x}) + u^r_{\rm SH}(\mathbf{x}) = 0, \quad & \mathbf{x} \in \Gamma^\xi, \\
\frac{\partial u^s_{\rm SH}}{\partial n}(\mathbf{x}) + \frac{\partial u^i}{\partial n}(\mathbf{x}) + \frac{\partial u^r_{\rm SH}}{\partial n}(\mathbf{x}) = 0, \quad & \mathbf{x} \in \Gamma_H, \\
\lim_{r\to\infty} \sqrt{r}\left(\frac{\partial u^s_{\rm SH}}{\partial r} - iku^s_{\rm SH}\right) = 0. &
\end{aligned} \tag{40}$$

The state problem is readily solved using the boundary integral equation (24). Once $\partial u^t_{\rm SH}/\partial n$ has been obtained on Γ^ξ, then the domain integral equation (16) can be used to recover $u^t_{\rm SH}$ (or $u^s_{\rm SH}$) anywhere within Ω^ξ (recall, $u^t_{\rm SH} = 0$ on Γ^ξ).

Next, we take the variation of $\mathcal{A}_{\rm SH}$ with respect to $u^s_{\rm SH}$. Using the divergence theorem and integration by parts, there results:

$$\begin{aligned}
\delta_{u^s_{\rm SH}}\mathcal{A}_{\rm SH} = \Re e\Bigg\{ & \int_{\Omega^\xi} \sum_{j=1}^{N_s} \delta u^s \frac{\bar{u}^s_{\rm SH}}{|u^s_m|^2}\left(1 - \frac{|u^s_m|}{|u^s_{\rm SH}|}\right)\Delta_D \,\mathrm{d}\Omega^\xi + \int_{\Omega^\xi} \delta u^s(\Delta\lambda + k^2\lambda)\mathrm{d}\Omega^\xi \\
& - \int_{\Gamma^\xi} \delta u^s \left(\frac{\partial\lambda}{\partial n} + \lambda_D\right)\mathrm{d}\Gamma^\xi - \int_{\Gamma_H} \delta u^s \frac{\partial\lambda}{\partial n}\mathrm{d}\Gamma_H + \int_{\Gamma^\xi} \lambda\frac{\partial\delta u^s}{\partial n}\mathrm{d}\Gamma^\xi \\
& - \int_{\Gamma_\infty} \delta u^s \left(\frac{\partial\lambda}{\partial r} - ik\lambda\right)\mathrm{d}\Gamma_\infty \Bigg\} = 0,
\end{aligned} \tag{41}$$

where an overbar ($\bar{u}^{\rm s}_{\rm SH}$) denotes complex conjugate of the subjugated quantity, and $\Delta_D \equiv \Delta_D(\mathbf{x} - \mathbf{x}_j)$ denotes the two-dimensional Dirac function. For arbitrary δu^s, Eq. (41) yields the strong form of the adjoint problem:

Adjoint problem:

$$\begin{aligned}
\Delta\lambda(\mathbf{x}) + k^2\lambda(\mathbf{x}) = -\sum_{j=1}^{N_s} \frac{\bar{u}^{\rm s}(\mathbf{x})}{|u^s_m(\mathbf{x}_j)|^2}\left(1 - \frac{|u^s_m(\mathbf{x}_j)|}{|u^s_{\rm SH}(\mathbf{x})|}\right)\Delta_D(\mathbf{x} - \mathbf{x}_j), \quad & \mathbf{x} \in \Omega^\xi, \\
\lambda(\mathbf{x}) = 0, \quad \lambda_D(\mathbf{x}) = -\frac{\partial\lambda}{\partial n}, \quad & \mathbf{x} \in \Gamma^\xi, \\
\frac{\partial\lambda}{\partial n}(\mathbf{x}) = 0, \quad & \mathbf{x} \in \Gamma_H, \\
\lim_{r\to\infty} \sqrt{r}\left(\frac{\partial\lambda}{\partial r} - ik\lambda\right) = 0. &
\end{aligned} \tag{42}$$

Notice that the governing operators of the state and adjoint problems are identical, and therefore one can use the same Green's function for both problems. Thus, borrowing from

the state problem, the boundary integral equation for the adjoint problem becomes:

$$S\left[\frac{\partial\lambda}{\partial n}\right](\mathbf{x}) = -\sum_{j=1}^{N_s} G^H_{\mathrm{SH}}(\mathbf{x},\mathbf{x}_j)\frac{\bar{u}^s_{\mathrm{SH}}(\mathbf{x}_j)}{|u^s_m(\mathbf{x}_j)|^2}\left(1-\frac{|u^s_m(\mathbf{x}_j)|}{|u^s_{\mathrm{SH}}(\mathbf{x}_j)|}\right), \quad \mathbf{x}\in\Gamma^\xi. \tag{43}$$

Next, we take the variation of $\mathcal{A}_{\mathrm{SH}}$ with respect to the parameter ξ, and make use of the total differentiation expressions derived earlier. Accordingly:

$$\begin{aligned}\delta_\xi\mathcal{A}_{\mathrm{SH}} = \frac{D}{D\xi}\Bigg[&\frac{1}{2}\sum_{j=1}^{N_s}\frac{\{|u^s_{\mathrm{SH}}(\mathbf{x}_j,\xi)|-|u^s_m(\mathbf{x}_j)|\}^2}{|u^s_m(\mathbf{x}_j)|^2} + \Re e\Bigg\{\int_{\Omega^\xi}\lambda(\Delta u^s_{\mathrm{SH}}+k^2u^s_{\mathrm{SH}})\mathrm{d}\Omega^\xi\\ &-\int_{\Gamma^\xi}\lambda_D(u^s_{\mathrm{SH}}+u^i+u^r_{\mathrm{SH}})\mathrm{d}\Gamma^\xi - \int_{\Gamma_H}\lambda\left(\frac{\partial u^s_{\mathrm{SH}}}{\partial n}+\frac{\partial u^i}{\partial n}+\frac{\partial u^r_{\mathrm{SH}}}{\partial n}\right)\mathrm{d}\Gamma_H\\ &-\int_{\Gamma_\infty}\lambda\left(\frac{\partial u^s_{\mathrm{SH}}}{\partial n}-iku^s_{\mathrm{SH}}\right)\mathrm{d}\Gamma_\infty\Bigg\}\Bigg]_{\xi=0}.\end{aligned} \tag{44}$$

Using the total derivative of a scalar field (34), and the fact that the normal component of the transformation velocity v_n vanishes at the N_s stations, since Γ_H does not change when Γ^ξ evolves, there results:

$$\begin{aligned}&\left[\frac{D}{D\xi}\left\{\frac{1}{2}\sum_{j=1}^{N_s}\frac{\{|u^s_{\mathrm{SH}}(\mathbf{x}_j,\xi)|-|u^s_m(\mathbf{x}_j)|\}^2}{|u^s_m(\mathbf{x}_j)|^2}\right\}\right]_{\xi=0}\\ &\quad= \Re e\left\{\sum_{j=1}^{N_s}\dot{u}^s_{\mathrm{SH}}(\mathbf{x}_j)\frac{\bar{u}^s_{\mathrm{SH}}(\mathbf{x}_j)}{|u^s_m(\mathbf{x}_j)|^2}\left(1-\frac{|u^s_m(\mathbf{x}_j)|}{|u^s_{\mathrm{SH}}(\mathbf{x}_j)|}\right)\right\}.\end{aligned} \tag{45}$$

Using (45), the divergence theorem, integration by parts, and the identity $\lambda\Delta u^s_{\mathrm{SH}} - \nabla\cdot(\lambda\nabla u^s_{\mathrm{SH}}) = -\nabla\lambda\cdot\nabla u^s_{\mathrm{SH}}$, (44) can be rewritten as:

$$\begin{aligned}\delta_\xi\mathcal{A}_{\mathrm{SH}} = \Re e&\left\{\sum_{j=1}^{N_s}\dot{u}^s_{\mathrm{SH}}(\mathbf{x}_j)\frac{\bar{u}^s_{\mathrm{SH}}(\mathbf{x}_j)}{|u^s_m(\mathbf{x}_j)|^2}\left(1-\frac{|u^s_m(\mathbf{x}_j)|}{|u^s_{\mathrm{SH}}(\mathbf{x}_j)|}\right)\right\}\\ &+\frac{D}{D\xi}\Bigg[\Re e\Bigg\{\int_{\Omega^\xi}(-\nabla\lambda\cdot\nabla u^s_{\mathrm{SH}}+k^2\lambda u^s_{\mathrm{SH}})\mathrm{d}\Omega^\xi + \int_{\Gamma^\xi}\lambda\frac{\partial u^s_{\mathrm{SH}}}{\partial n}\mathrm{d}\Gamma^\xi\\ &-\int_{\Gamma^\xi}\lambda_D(u^s_{\mathrm{SH}}+u^i+u^r_{\mathrm{SH}})\mathrm{d}\Gamma^\xi - \int_{\Gamma_H}\lambda\left(\frac{\partial u^i}{\partial n}+\frac{\partial u^r_{\mathrm{SH}}}{\partial n}\right)\mathrm{d}\Gamma_H\\ &+\int_{\Gamma_\infty}\lambda ik\,u^s_{\mathrm{SH}}\mathrm{d}\Gamma_\infty\Bigg\}\Bigg]_{\xi=0}.\end{aligned} \tag{46}$$

Next, using (35), the total derivative of the line integrals over Γ^ξ in (46) can be expressed as:

$$\frac{D}{D\xi}\left[\Re e\int_{\Gamma^\xi}\lambda\frac{\partial u^s_{\rm SH}}{\partial n}\mathrm{d}\Gamma^\xi\right]_{\xi=0}=\Re e\int_{\Gamma_S}\left[\dot\lambda\frac{\partial u^s_{\rm SH}}{\partial n}+v_n\frac{\partial\lambda}{\partial n}\frac{\partial u^s_{\rm SH}}{\partial n}\right]\mathrm{d}\Gamma, \quad (47)$$

$$\frac{D}{D\xi}\left[\Re e\int_{\Gamma^\xi}\lambda_D(u^s_{\rm SH}+u^i+u^r_{\rm SH})\mathrm{d}\Gamma^\xi\right]_{\xi=0}=\Re e\int_{\Gamma_S}\left[\lambda_D\dot u^t_{\rm SH}+v_n\lambda_D\frac{\partial u^t_{\rm SH}}{\partial n}\right]\mathrm{d}\Gamma, \quad (48)$$

where it should be noted that $\dot\lambda$ and $\partial\lambda/\partial n$ in (47), and $\dot u^t_{\rm SH}$ and $\partial u^t_{\rm SH}/\partial n$ in (48) do not vanish even though λ and $u^t_{\rm SH}$ vanish on Γ_S. We remark that the boundary segments Γ_∞ and Γ_H do not change by the evolution of Γ^ξ, that is, v_n vanishes on Γ_∞ and Γ_H. In addition, u^i and $u^r_{\rm SH}$ on Γ_H are independent of ξ so that $(\partial\dot u^i/\partial n)+(\partial\dot u^r_{\rm SH}/\partial n)$ vanishes on Γ_H. Therefore, the total derivative of the line integrals on Γ_H and Γ_∞ are:

$$\frac{D}{D\xi}\left[\Re e\int_{\Gamma_H}\lambda\left(\frac{\partial u^i}{\partial n}+\frac{\partial u^r_{\rm SH}}{\partial n}\right)\mathrm{d}\Gamma_H\right]_{\xi=0}=\Re e\int_{\Gamma_H}\left[\dot\lambda\left(\frac{\partial u^i}{\partial n}+\frac{\partial u^r_{\rm SH}}{\partial n}\right)\right]\mathrm{d}\Gamma_H=0, \quad (49)$$

$$\frac{D}{D\xi}\left[\Re e\int_{\Gamma_\infty}\lambda iku^s_{\rm SH}\mathrm{d}\Gamma_\infty\right]_{\xi=0}=\Re e\int_{\Gamma_\infty}ik(\lambda\dot u^s_{\rm SH})\mathrm{d}\Gamma_\infty, \quad (50)$$

where the boundary condition (7) was also used. Next, using (36), there results:

$$\begin{aligned}\frac{D}{D\xi}&\Re e\left[\left\{\int_{\Omega^\xi}(-\nabla\lambda\cdot\nabla u^s_{\rm SH}+k^2\lambda u^s_{\rm SH})\mathrm{d}\Omega^\xi\right\}\right]_{\xi=0}\\&=\Re e\Big\{\int_\Omega(-\nabla\dot\lambda\cdot\nabla u^s_{\rm SH}-\nabla\lambda\cdot\nabla\dot u^s_{\rm SH}+k^2\dot\lambda u^s_{\rm SH}+k^2\lambda\dot u^s_{\rm SH})\mathrm{d}\Omega\\&\quad+\int_{\Gamma_S}(-\nabla\lambda\cdot\nabla u^s_{\rm SH})v_n\mathrm{d}\Gamma\Big\}. \quad (51)\end{aligned}$$

By virtue of (47)–(51), (46) can now be cast as:

$$\begin{aligned}\delta_\xi\mathcal{A}_{\rm SH}=\Re e&\left\{\sum_{j=1}^{N_s}\dot u^s_{\rm SH}(\mathbf{x}_j)\frac{\bar u^s_{\rm SH}(\mathbf{x}_j)}{|u^s_m(\mathbf{x}_j)|^2}\left(1-\frac{|u^s_m(\mathbf{x}_j)|}{|u^s_{\rm SH}(\mathbf{x}_j)|}\right)\right\}\\&+\Re e\Big[\int_\Omega(-\nabla\dot\lambda\cdot\nabla u^s_{\rm SH}-\nabla\lambda\cdot\nabla\dot u^s_{\rm SH}+k^2\dot\lambda u^s_{\rm SH}+k^2\lambda\dot u^s_{\rm SH})\mathrm{d}\Omega\\&+\int_{\Gamma_S}(-\nabla\lambda\cdot\nabla u^s_{\rm SH})v_n\mathrm{d}\Gamma+\int_{\Gamma_S}\dot\lambda\frac{\partial u^s_{\rm SH}}{\partial n}\mathrm{d}\Gamma+\int_{\Gamma_S}v_n\frac{\partial\lambda}{\partial n}\frac{\partial u^s_{\rm SH}}{\partial n}\mathrm{d}\Gamma\\&-\int_{\Gamma_S}\lambda_D\dot u^t_{\rm SH}\mathrm{d}\Gamma-\int_{\Gamma_S}v_n\lambda_D\frac{\partial u^t_{\rm SH}}{\partial n}\mathrm{d}\Gamma+\int_{\Gamma_\infty}ik(\lambda\dot u^s_{\rm SH})\mathrm{d}\Gamma\Big]. \quad (52)\end{aligned}$$

The following relationships can be used to simplify (52):

$$\int_{\Omega}(-\nabla\dot{\lambda}\cdot\nabla u^s_{\mathrm{SH}}+\dot{\lambda}k^2u^s_{\mathrm{SH}})\mathrm{d}\Omega+\int_{\Gamma_S}\dot{\lambda}\frac{\partial u^s_{\mathrm{SH}}}{\partial n}\mathrm{d}\Gamma+\int_{\Gamma_\infty}ik\dot{\lambda}u^s_{\mathrm{SH}}\mathrm{d}\Gamma_\infty=0, \tag{53}$$

$$\int_{\Omega}(-\nabla\dot{u}^s_{\mathrm{SH}}\cdot\nabla\lambda+\dot{u}^s_{\mathrm{SH}}k^2\lambda)\mathrm{d}\Omega+\sum_{j=1}^{N_s}\dot{u}^s_{\mathrm{SH}}(\mathbf{x}_j)\frac{\bar{u}^s_{\mathrm{SH}}(\mathbf{x}_j)}{|u^s_m(\mathbf{x}_j)|^2}\left(1-\frac{|u^s_m(\mathbf{x}_j)|}{|u^s_{\mathrm{SH}}(\mathbf{x}_j)|}\right)$$
$$+\int_{\Gamma_\infty}ik\dot{u}^s_{\mathrm{SH}}\lambda\mathrm{d}\Gamma_\infty+\int_{\Gamma_S}\dot{u}^s_{\mathrm{SH}}\frac{\partial\lambda}{\partial n}\mathrm{d}\Gamma=0, \tag{54}$$

where (53) and (54) are the weak forms of the state and adjoint problems, with $\dot{u}^s_{\mathrm{SH}}$ and $\dot{\lambda}$ acting as weight functions, respectively. Thus, (52) is reduced to:

$$\delta_\xi\mathcal{A}_{\mathrm{SH}}=\Re e\left[\int_{\Gamma_S}(-\nabla\lambda\cdot\nabla u^s_{\mathrm{SH}})v_n\mathrm{d}\Gamma-\int_{\Gamma_S}\dot{u}^s_{\mathrm{SH}}\frac{\partial\lambda}{\partial n}\mathrm{d}\Gamma-\int_{\Gamma_S}\lambda_D\dot{u}^t_{\mathrm{SH}}\mathrm{d}\Gamma\right.$$
$$\left.+\int_{\Gamma_S}v_n\frac{\partial\lambda}{\partial n}\frac{\partial u^s_{\mathrm{SH}}}{\partial n}\mathrm{d}\Gamma-\int_{\Gamma_S}v_n\lambda_D\frac{\partial u^t_{\mathrm{SH}}}{\partial n}\mathrm{d}\Gamma\right]. \tag{55}$$

Next using the decomposition of a gradient into its tangential and normal components, the following holds:

$$-\nabla\lambda\cdot\nabla u^s_{\mathrm{SH}}=-\left(\frac{\partial\lambda}{\partial s}\mathbf{t}+\frac{\partial\lambda}{\partial n}\mathbf{n}\right)\cdot\left(\frac{\partial u^s_{\mathrm{SH}}}{\partial s}\mathbf{t}+\frac{\partial u^s_{\mathrm{SH}}}{\partial n}\mathbf{n}\right)\quad\text{on }\Gamma_S, \tag{56}$$

where $\mathbf{t}$ denotes the unit tangential vector on Γ_S, and s denotes arc-length. Since $\partial\lambda/\partial s$ vanishes on Γ_S ($\lambda=0$ on Γ_S, per (42)), and $\mathbf{n}\cdot\mathbf{t}=0$, (56) becomes:

$$-\nabla\lambda\cdot\nabla u^s_{\mathrm{SH}}=-\frac{\partial\lambda}{\partial n}\frac{\partial u^s_{\mathrm{SH}}}{\partial n}\quad\text{on }\Gamma_S. \tag{57}$$

With the aid of (57) and the fact that $\dot{u}^i$ and $\dot{u}^r_{\mathrm{SH}}$ vanish, (55) reduces to:

$$\delta_\xi\mathcal{A}_{\mathrm{SH}}=\Re e\left[\int_{\Gamma_S}v_n\frac{\partial\lambda}{\partial n}\frac{\partial u^t_{\mathrm{SH}}}{\partial n}\mathrm{d}\Gamma\right]. \tag{58}$$

Requiring (58) to vanish yields the control problem.

Control problem:

$$\delta_\xi\mathcal{A}_{\mathrm{SH}}=\Re e\left[\int_{\Gamma_S}v_n\frac{\partial\lambda}{\partial n}\frac{\partial u^t_{\mathrm{SH}}}{\partial n}\mathrm{d}\Gamma\right]=0. \tag{59}$$

In (59), $\partial u^t_{\mathrm{SH}}/\partial n$ and $\partial\lambda/\partial n$ are, respectively, the solutions of (24) and (43). The state problem (40), the adjoint problem (42), and the control problem (59) constitute the backbone of the inverse problem. The iterative solution of all three problems allows for the determination of the location and the shape of the sought scatterer.

4.3. *Acoustic case*

4.3.1. *Augmented misfit functional*

In the acoustic case, the misfit is defined based on the difference of the absolute values of Neumann data, i.e. $|\partial u^s_{\rm AC}/\partial n|$ and $|\partial u^s_m/\partial n|$ on the free surface. The augmented functional, resulting from the side imposition of (9)–(12), is:

$$\begin{aligned}\mathcal{A}_{\rm AC}(u^s_{\rm AC},\lambda,\xi) = \frac{1}{2}\sum_{j=1}^{N_s}\frac{\left\{\left|\frac{\partial u^s_{\rm AC}}{\partial n}(\mathbf{x}_j,\xi)\right| - \left|\frac{\partial u^s_m}{\partial n}(\mathbf{x}_j)\right|\right\}^2}{\left|\frac{\partial u^s_m}{\partial n}(\mathbf{x}_j)\right|^2}\\ + \Re e\Bigg\{\int_{\Omega^\xi}\lambda(\mathbf{x}^\xi,\xi)[\Delta u^s_{\rm AC}(\mathbf{x}^\xi,\xi)+k^2u^s_{\rm AC}(\mathbf{x}^\xi,\xi)]\mathrm{d}\Omega^\xi\\ - \int_{\Gamma^\xi}\lambda(\mathbf{x}^\xi,\xi)\left[\frac{\partial u^s_{\rm AC}}{\partial n}(\mathbf{x}^\xi,\xi)+\frac{\partial u^i}{\partial n}(\mathbf{x}^\xi)+\frac{\partial u^r_{\rm AC}}{\partial n}(\mathbf{x}^\xi)\right]\mathrm{d}\Gamma^\xi\\ - \int_{\Gamma_H}\lambda_D(\mathbf{x}^\xi,\xi)[u^s_{\rm AC}(\mathbf{x}^\xi,\xi)+u^i(\mathbf{x}^\xi)+u^r_{\rm AC}(\mathbf{x}^\xi)]\mathrm{d}\Gamma_H\\ - \int_{\Gamma_\infty}\lambda(\mathbf{x}^\xi,\xi)\left[\frac{\partial u^s_{\rm AC}}{\partial r}(\mathbf{x}^\xi,\xi)-iku^s_{\rm AC}(\mathbf{x}^\xi,\xi)\right]\mathrm{d}\Gamma_\infty\Bigg\}. \end{aligned} \tag{60}$$

4.3.2. *The first-order optimality conditions*

We impose stationarity of the augmented functional (60) by requiring that its first variation vanish. Similarly to the SH case, the vanishing of the variations of $\mathcal{A}_{\rm AC}$ with respect to the adjoint variables λ and λ_D for arbitrary $\delta\lambda$ and $\delta\lambda_D$ recovers the strong form of the state problem given by (9)–(12). We use the boundary integral equation (29) to solve for the state variables $u^t_{\rm AC}$. Once $u^t_{\rm AC}$ has been obtained on Γ^ξ, then the domain integral equation (25) can be used to recover $u^t_{\rm AC}$ anywhere within Ω^ξ.

The second optimality condition is obtained by requiring that the variation of the augmented functional $\mathcal{A}_{\rm AC}$ with respect to the state variable $u^s_{\rm AC}$ vanish. There results:

$$\begin{aligned}\delta_{u^s_{\rm AC}}\mathcal{A}_{\rm AC} = \Re e\Bigg\{\int_{\Omega^\xi}\sum_{j=1}^{N_s}\frac{\partial\delta u^s}{\partial n}\frac{\overline{\frac{\partial u^s_{\rm AC}}{\partial n}}}{\left|\frac{\partial u^s_m}{\partial n}\right|^2}\left(1-\frac{\left|\frac{\partial u^s_m}{\partial n}\right|}{\left|\frac{\partial u^s_{\rm AC}}{\partial n}\right|}\right)\Delta_D\,\mathrm{d}\Omega^\xi\\ + \int_{\Omega^\xi}\delta u^s(\Delta\lambda+k^2\lambda)\mathrm{d}\Omega^\xi - \int_{\Gamma_H}\delta u^s\left(\frac{\partial\lambda}{\partial n}+\lambda_D\right)\mathrm{d}\Gamma_H - \int_{\Gamma^\xi}\delta u^s\frac{\partial\lambda}{\partial n}\mathrm{d}\Gamma^\xi\\ + \int_{\Gamma_H}\lambda\frac{\partial\delta u^s}{\partial n}\mathrm{d}\Gamma_H - \int_{\Gamma_\infty}\delta u^s\left(\frac{\partial\lambda}{\partial n}-ik\lambda\right)\mathrm{d}\Gamma_\infty\Bigg\} = 0. \end{aligned} \tag{61}$$

For arbitrary $\partial\delta u^s/\partial n$ on Γ_H, and arbitrary δu^s, from (61) we obtain:

Adjoint problem:

$$\begin{aligned}
\Delta\lambda(\mathbf{x}) + k^2\lambda(\mathbf{x}) &= 0, \quad \mathbf{x} \in \Omega^\xi,\\
\lambda(\mathbf{x}) = -\sum_{j=1}^{N_s} \frac{\overline{\dfrac{\partial u^s_{\mathrm{AC}}}{\partial n}}(\mathbf{x})}{\left|\dfrac{\partial u^s_m}{\partial n}(\mathbf{x}_j)\right|^2} \left(1 - \frac{\left|\dfrac{\partial u^s_m}{\partial n}(\mathbf{x}_j)\right|}{\left|\dfrac{\partial u^s_{\mathrm{AC}}}{\partial n}(\mathbf{x})\right|}\right) \Delta_D(\mathbf{x}-\mathbf{x}_j), \quad \lambda_D(\mathbf{x}) &= -\frac{\partial\lambda}{\partial n}(\mathbf{x}), \quad \mathbf{x} \in \Gamma_H,\\
\frac{\partial\lambda}{\partial n}(\mathbf{x}) &= 0, \quad \mathbf{x} \in \Gamma^\xi,\\
\lim_{r\to\infty} \sqrt{r}\left(\frac{\partial\lambda}{\partial r} - ik\lambda\right) &= 0.
\end{aligned} \tag{62}$$

Since the adjoint problem is also governed by the Helmholtz operator, the problem can also be solved numerically using the following boundary integral equation:

$$\frac{1}{2}\lambda(\mathbf{x}) - D[\lambda](\mathbf{x}) = -\sum_{j=1}^{N_s} \frac{\overline{\dfrac{\partial u^s_{\mathrm{AC}}}{\partial n}}(\mathbf{x}_j)}{\left|\dfrac{\partial u^s_m}{\partial n}(\mathbf{x}_j)\right|^2} \left(1 - \frac{\left|\dfrac{\partial u^s_m}{\partial n}(\mathbf{x}_j)\right|}{\left|\dfrac{\partial u^s_{\mathrm{AC}}}{\partial n}(\mathbf{x}_j)\right|}\right) \frac{\partial G^H_{\mathrm{AC}}(\mathbf{x},\mathbf{x}_j)}{\partial n_{\mathbf{x}_j}}, \quad \mathbf{x} \in \Gamma^\xi. \tag{63}$$

Lastly, the third optimality condition results from the variations of the augmented functional with respect to ξ; there results:

$$\begin{aligned}
\delta_\xi \mathcal{A}_{\mathrm{AC}} = \frac{D}{D\xi}\Bigg[& \frac{1}{2}\sum_{j=1}^{N_s} \frac{\left\{\left|\dfrac{\partial u^s_{\mathrm{AC}}}{\partial n}(\mathbf{x}_j,\xi)\right| - \left|\dfrac{\partial u^s_m}{\partial n}(\mathbf{x}_j)\right|\right\}^2}{\left|\dfrac{\partial u^s_m}{\partial n}(\mathbf{x}_j)\right|^2}\\
& + \Re e\left\{\int_{\Omega^\xi} \lambda(\Delta u^s_{\mathrm{AC}} + k^2 u^s_{\mathrm{AC}})\mathrm{d}\Omega^\xi - \int_{\Gamma^\xi} \lambda\left(\frac{\partial u^s_{\mathrm{AC}}}{\partial n} + \frac{\partial u^i}{\partial n} + \frac{\partial u^r_{\mathrm{AC}}}{\partial n}\right)\mathrm{d}\Gamma^\xi\right.\\
& \left. - \int_{\Gamma_H} \lambda_D(u^s_{\mathrm{AC}} + u^i + u^r_{\mathrm{AC}})\mathrm{d}\Gamma_H - \int_{\Gamma_\infty} \lambda\left(\frac{\partial u^s_{\mathrm{AC}}}{\partial n} - iku^s_{\mathrm{AC}}\right)\mathrm{d}\Gamma\right\}\Bigg]_{\xi=0}.
\end{aligned} \tag{64}$$

The first term in (64) can be further simplified by using the total derivative of a scalar field; accordingly:

$$\left[\frac{D}{D\xi}\left\{\frac{1}{2}\sum_{j=1}^{N_s} \frac{\left\{\left|\dfrac{\partial u^s_{\mathrm{AC}}}{\partial n}(\mathbf{x}_j,\xi)\right| - \left|\dfrac{\partial u^s_m}{\partial n}(\mathbf{x}_j)\right|\right\}^2}{\left|\dfrac{\partial u^s_m}{\partial n}(\mathbf{x}_j)\right|^2}\right\}\right]_{\xi=0}$$

$$= \Re e\left\{\sum_{j=1}^{N_s} \frac{\partial \dot{u}^s_{\rm AC}}{\partial n}(\mathbf{x}_j) \frac{\overline{\frac{\partial u^s_{\rm AC}}{\partial n}}(\mathbf{x}_j)}{\left|\frac{\partial u^s_m}{\partial n}(\mathbf{x}_j)\right|^2}\left(1 - \frac{\left|\frac{\partial u^s_m}{\partial n}(\mathbf{x}_j)\right|}{\left|\frac{\partial u^s_{\rm AC}}{\partial n}(\mathbf{x}_j)\right|}\right)\right\}. \tag{65}$$

By virtue of (65), the divergence theorem, and integration by parts, (64) yields:

$$\begin{aligned}\delta_\xi \mathcal{A}_{\rm AC} = \Re e\Bigg\{&\sum_{j=1}^{N_s} \frac{\partial \dot{u}^s_{\rm AC}}{\partial n}(\mathbf{x}_j) \frac{\overline{\frac{\partial u^s_{\rm AC}}{\partial n}}(\mathbf{x}_j)}{\left|\frac{\partial u^s_m}{\partial n}(\mathbf{x}_j)\right|^2}\left(1 - \frac{\left|\frac{\partial u^s_m}{\partial n}(\mathbf{x}_j)\right|}{\left|\frac{\partial u^s_{\rm AC}}{\partial n}(\mathbf{x}_j)\right|}\right)\Bigg\}\\ &+ \frac{D}{D\xi}\Bigg[\Re e\Bigg\{\int_{\Omega^\xi}(-\nabla\lambda\cdot\nabla u^s_{\rm AC} + k^2\lambda u^s_{\rm AC})\mathrm{d}\Omega^\xi\\ &- \int_{\Gamma^\xi}\lambda\left(\frac{\partial u^i}{\partial n} + \frac{\partial u^r_{\rm AC}}{\partial n}\right)\mathrm{d}\Gamma^\xi - \int_{\Gamma_H}\lambda_D\left(u^s_{\rm AC} + u^i + u^r_{\rm AC}\right)\mathrm{d}\Gamma_H\\ &+ \int_{\Gamma_H}\lambda\frac{\partial u^s_{\rm AC}}{\partial n}\mathrm{d}\Gamma_H + \int_{\Gamma_\infty}\lambda iku^s_{\rm AC}\mathrm{d}\Gamma_\infty\Bigg\}\Bigg]_{\xi=0}.\end{aligned} \tag{66}$$

It can also be shown that[1]:

$$\frac{\partial}{\partial\xi}\left(\frac{\partial u^i}{\partial n}\right) = -\frac{\partial u^i}{\partial s}\frac{\partial v_n}{\partial s} + v_n\frac{\partial u^i}{\partial s}\mathrm{div}\,\mathbf{t} \quad \text{on } \Gamma_{\rm S}. \tag{67}$$

Equation (67) holds also if u^i were to be replaced by $u^r_{\rm AC}$. Moreover, the Helmholtz equation can be expressed in terms of u^i or $u^r_{\rm AC}$ in a tangential-normal coordinate system, per:

$$\begin{aligned}\frac{\partial^2 u^i}{\partial n^2} - \kappa\frac{\partial u^i}{\partial n} + \frac{\partial^2 u^i}{\partial s^2} + k^2 u^i = 0,\\ \frac{\partial^2 u^r_{\rm AC}}{\partial n^2} - \kappa\frac{\partial u^r_{\rm AC}}{\partial n} + \frac{\partial^2 u^r_{\rm AC}}{\partial s^2} + k^2 u^r_{\rm AC} = 0.\end{aligned} \tag{68}$$

Thus, by using (35), (67), and (68), the total derivative of the line integral over Γ^ξ is derived as follows:

$$\begin{aligned}&\frac{D}{D\xi}\left[\Re e\int_{\Gamma^\xi}\lambda\left(\frac{\partial u^i}{\partial n} + \frac{\partial u^r_{\rm AC}}{\partial n}\right)\mathrm{d}\Gamma^\xi\right]_{\xi=0}\\ &\quad= \Re e\int_{\Gamma_S}\Bigg[-\dot{\lambda}\frac{\partial u^s_{\rm AC}}{\partial n} - \lambda v_n\frac{\partial^2(u^i + u^r_{\rm AC})}{\partial s^2} - k^2\lambda v_n(u^i + u^r_{\rm AC})\\ &\qquad- \lambda\frac{\partial v_n}{\partial s}\left(\frac{\partial u^i}{\partial s} + \frac{\partial u^r_{\rm AC}}{\partial s}\right) + \lambda v_n\left(\frac{\partial u^i}{\partial s} + \frac{\partial u^r_{\rm AC}}{\partial s}\right)\mathrm{div}\,\mathbf{t}\Bigg]\mathrm{d}\Gamma.\end{aligned} \tag{69}$$

The total derivative of the line integral over Γ_H is:

$$\frac{D}{D\xi}\left[\Re e\int_{\Gamma_H}\lambda_D(u^s_{\rm AC}+u^i+u^r_{\rm AC})\mathrm{d}\Gamma_H\right]_{\xi=0}=-\Re e\int_{\Gamma_H}\frac{\partial\lambda}{\partial n}\dot{u}^s_{\rm AC}\mathrm{d}\Gamma_H, \tag{70}$$

$$\frac{D}{D\xi}\left[\Re e\int_{\Gamma_H}\lambda\frac{\partial u^s_{\rm AC}}{\partial n}\mathrm{d}\Gamma_H\right]_{\xi=0}=\Re e\int_{\Gamma_H}\left[\dot{\lambda}\frac{\partial u^s_{\rm AC}}{\partial n}+\lambda\frac{\partial\dot{u}^s_{\rm AC}}{\partial n}\right]\mathrm{d}\Gamma_H. \tag{71}$$

The total derivative of the line integral over Γ_∞ is:

$$\frac{D}{D\xi}\left[\Re e\int_{\Gamma_\infty}ik\lambda u^s_{\rm AC}\mathrm{d}\Gamma_\infty\right]_{\xi=0}=\Re e\int_{\Gamma_\infty}ik(\dot{\lambda}u^s_{\rm AC}+\lambda\dot{u}^s_{AC})\mathrm{d}\Gamma_\infty. \tag{72}$$

Based on (36), the total derivative of the domain integral over Ω^ξ becomes:

$$\begin{aligned}\frac{D}{D\xi}\Re e\left\{\int_{\Omega^\xi}(-\nabla\lambda\cdot\nabla u^s_{\rm AC}+k^2\lambda u^s_{\rm AC})\mathrm{d}\Omega^\xi\right\}\\ =\Re e\left\{\int_\Omega(-\nabla\dot{\lambda}\cdot\nabla u^s_{\rm AC}-\nabla\lambda\cdot\nabla\dot{u}^s_{\rm AC}+k^2\dot{\lambda}u^s_{\rm AC}+k^2\lambda\dot{u}^s_{\rm AC})\mathrm{d}\Omega\right.\\ \left.+\int_{\Gamma_S}(-\nabla\lambda\cdot\nabla u^s_{\rm AC}+k^2\lambda u^s_{\rm AC})v_n\mathrm{d}\Gamma\right\}.\end{aligned} \tag{73}$$

Using next the boundary condition on Γ_H of the adjoint problem (see (62), the following holds:

$$\int_{\Gamma_H}\lambda\frac{\partial\dot{u}^s}{\partial n}\mathrm{d}\Gamma=-\sum_{j=1}^{N_s}\frac{\partial\dot{u}^s_{\rm AC}}{\partial n}(\mathbf{x}_j)\frac{\overline{\frac{\partial u^s_{\rm AC}}{\partial n}}(\mathbf{x}_j)}{\left|\frac{\partial u^s_m}{\partial n}(\mathbf{x}_j)\right|^2}\left(1-\frac{\left|\frac{\partial u^s_m}{\partial n}(\mathbf{x}_j)\right|}{\left|\frac{\partial u^s_{\rm AC}}{\partial n}(\mathbf{x}_j)\right|}\right). \tag{74}$$

By substituting the above total derivatives of the line and domain integrals (69)–(74) into (66), and with the aid of appropriate weak forms of the state and adjoint problems (using $\dot{\lambda}$ and $\dot{u}^s_{\rm AC}$ as weight functions, respectively), (66) reduces to:

$$\begin{aligned}\delta_\xi\mathcal{A}_{\rm AC}=\Re e\left[\int_{\Gamma_S}\left\{(-\nabla\lambda\cdot\nabla u^s_{\rm AC}+k^2\lambda u^t_{\rm AC})v_n+\lambda v_n\frac{\partial^2(u^i+u^r_{\rm AC})}{\partial s^2}\right.\right.\\ \left.\left.+\lambda\frac{\partial v_n}{\partial s}\left(\frac{\partial u^i}{\partial s}+\frac{\partial u^r_{\rm AC}}{\partial s}\right)-\lambda v_n\left(\frac{\partial u^i}{\partial s}+\frac{\partial u^r_{\rm AC}}{\partial s}\right)\mathrm{div}\,\mathbf{t}\right\}\mathrm{d}\Gamma\right].\end{aligned} \tag{75}$$

Using the decomposition of a gradient, there holds:

$$-\nabla\lambda\cdot\nabla u^s_{\rm AC}=-\frac{\partial\lambda}{\partial s}\frac{\partial u^s_{\rm AC}}{\partial s}\quad\text{on }\Gamma_S. \tag{76}$$

Therefore, (75) becomes:

$$\delta_\xi \mathcal{A}_{\rm AC} = \Re e \int_{\Gamma_S} \left[v_n \left\{ -\frac{\partial \lambda}{\partial s} \frac{\partial u^s_{\rm AC}}{\partial s} + \lambda \frac{\partial^2 (u^i + u^r_{\rm AC})}{\partial s^2} + k^2 \lambda u^t_{\rm AC} \right\} \right.$$
$$\left. + \lambda \frac{\partial v_n}{\partial s} \left(\frac{\partial u^i}{\partial s} + \frac{\partial u^r_{\rm AC}}{\partial s} \right) - \lambda v_n \left(\frac{\partial u^i}{\partial s} + \frac{\partial u^r_{\rm AC}}{\partial s} \right) \operatorname{div} \mathbf{t} \right] \mathrm{d}\Gamma. \tag{77}$$

Using integration by parts, there holds:

$$\int_\Gamma \left\{ v_n \lambda \frac{\partial^2 (u^i + u^r_{\rm AC})}{\partial s^2} \right\} \mathrm{d}\Gamma = \left[v_n \lambda \frac{\partial (u^i + u^r_{\rm AC})}{\partial s} \right]_{\Gamma_S} - \int_{\Gamma_S} \left\{ \frac{\partial}{\partial s} (v_n \lambda) \frac{\partial (u^i + u^r_{\rm AC})}{\partial s} \right\} \mathrm{d}\Gamma$$
$$= - \int_{\Gamma_S} \left\{ \left(\frac{\partial v_n}{\partial s} \lambda + \frac{\partial \lambda}{\partial s} v_n \right) \frac{\partial (u^i + u^r_{\rm AC})}{\partial s} \right\} \mathrm{d}\Gamma. \tag{78}$$

Using the above, the vanishing of (77) gives rise to the control problem.

Control problem:

$$\delta_\xi \mathcal{A}_{\rm AC} = \Re e \int_{\Gamma_S} v_n \left\{ -\frac{\partial \lambda}{\partial s} \frac{\partial u^t_{\rm AC}}{\partial s} + k^2 \lambda u^t_{\rm AC} - \lambda \frac{\partial (u^i + u^r_{\rm AC})}{\partial s} \operatorname{div} \mathbf{t} \right\} \mathrm{d}\Gamma = 0. \tag{79}$$

We note that the tangential derivatives terms appearing in the control problem (79) are implemented, upon discretization, by using the first derivative of the shape functions with respect to arc-length.

5. Numerical Experiments

For both the SH and the acoustic cases, satisfaction of the KKT system resulting from the discretization of the state, adjoint, and control problems, will ensure the stationarity of the augmented functionals $\mathcal{A}_{\rm SH}$ and $\mathcal{A}_{\rm AC}$, respectively. This, in turn, leads (hopefully) to the localization and shape reconstruction of the target. To resolve the triad of the state, adjoint, and control problems, one could simultaneously solve for the state variables, the adjoint variables, and the shape parameters embedded in the control problem, by using a full-space solution approach. Here, however, we opt for a reduced-space approach, whereby the state and adjoint variables are projected to the space of the shape parameters. In brief, first the state problem is solved using the discrete counterpart of integral equation (24) or (29), thus yielding the state variables $u^s_{\rm SH}$ or $u^s_{\rm AC}$, respectively. Then, the adjoint problem is solved, using the misfit as a driver, and integral equations (43) or (63), respectively, thus yielding the adjoint variables λ. Finally, we use the control problem ((59) or (79)) to drive the shape iterations, until convergence. We remark that every component of the gradient of the misfit functional with respect to a shape parameter is equal to the variation of the misfit functional with respect to the shape metric. That is:

$$\delta_{p_i} \mathcal{A} = \nabla_{p_i} \mathcal{L}, \tag{80}$$

where p_i denotes the ith model parameter (unknown). For example, for the SH case, (80) implies that (using also (59)):

$$\delta_{p_i}\mathcal{A} = \Re e\left[\int_{\Gamma_S} v_n^i \frac{\partial\lambda}{\partial n}\frac{\partial u_{\mathrm{SH}}^t}{\partial n} d\Gamma\right]. \tag{81}$$

Similarly, for the acoustic case, (80) implies that (using also (79)):

$$\delta_{p_i}\mathcal{A} = \Re e\left[\int_{\Gamma_S} v_n^i \left\{-\frac{\partial\lambda}{\partial s}\frac{\partial u_{\mathrm{AC}}^t}{\partial s} + k^2\lambda u_{\mathrm{AC}}^t - \lambda\frac{\partial(u^i + u_{\mathrm{AC}}^r)}{\partial s}\mathrm{div}\,\mathbf{t}\right\} \mathrm{d}\Gamma\right], \tag{82}$$

where v_n^i denotes the normal transformation velocity corresponding to the ith model parameter. Therefore, if we now seek to minimize the misfit $\mathcal{L}$, using any gradient-based scheme (e.g. conjugate-gradient), the components of the gradient of the misfit are readily given by (81) and (82), for the SH and acoustic cases, respectively, while at the same time both the state and adjoint problems have been satisfied. All that remains is to define the components of the transformation velocity v_n^i. To this end, let $\mathbf{\Psi}(\mathbf{p})$ denote the (vector) function describing the parameterization of the unknown boundary, in terms of a finite set of unknown parameters $\mathbf{p}$. Then, the transformation velocity at a point $\mathbf{x} \in \Gamma_S$ is defined as:

$$v_n^i(\mathbf{x}) = \left.\frac{\partial\mathbf{\Psi}(\mathbf{p})}{\partial p_i}\right|_{\mathrm{at}\,\mathbf{x}} \cdot \mathbf{n}(\mathbf{x}) = \frac{\partial\Psi_x}{\partial p_i}n_x + \frac{\partial\Psi_y}{\partial p_i}n_y, \tag{83}$$

where Ψ_x and Ψ_y are the cartesian components of the parameterization function $\mathbf{\Psi}$, and n_x, n_y are similarly the cartesian components of the normal vector.

Although the described process will ensure the stationarity of the augmented functionals, and thus the simultaneous satisfaction of the PDEs and the minimization of the misfit, there is no guarantee that the process will converge, or that it will converge to the true target. Typically, in full waveform-based inversion, regularization terms are added to the augmented functional in an attempt to narrow the solution feasibility space. Here, in lieu of regularization, we embed the inversion process within a frequency and directionality continuation scheme.[17] Specifically, we solve, a sequence of, seemingly, uncoupled problems corresponding to different probing frequencies and/or directions. For example: the inversion algorithm is initiated using, for example, a low probing frequency, and is let to converge (at whichever location/shape the optimizer drives the solution), before the converged solution is fed as initial guess to the next probing frequency. The process is repeated until all problems converge under the same set of shape parameters. The continuation scheme may be applied over frequencies, wave incidence directions, or both. It is typically sufficient to use only a few frequencies and/or directions for convergence.

From a practical perspective, it appears that low probing frequencies are typically capable of resolving location, whereas higher frequencies are needed to refine the shape. Motivated by the latter observation and to further aid the reconstruction process, we also implemented a scheme according to which the shape remains simple and constrained (e.g. circular) until there is no significant movement, and then the constraint is released to allow for shape refinement.

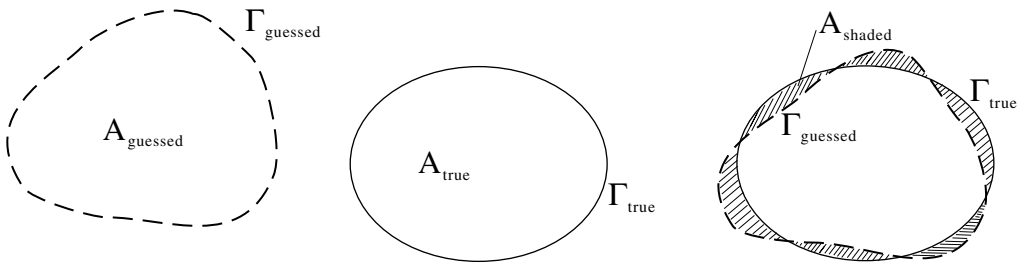

(a) Case 1: Shape estimate does not overlap with the true target

(b) Case 2: Shape estimate partially overlaps with the true target

Fig. 5. Solution-fitness e_f definitions.

We discuss next numerical results of detecting the shape and location of a circular, elliptical, potato-shaped, and kite-shaped scatterers. In all example problems, the measured data are synthesized numerically by solving the forward problem using the boundary element method with a mesh different from the one we use in the inversion process in order to avoid committing a classical inverse crime. We show the convergence path of the shapes with respect to the number of inversion iterations, and measure also the solution-fitness e_f by computing the normalized area-difference delineated by the mismatch between the boundaries of the guessed scatterer and the true target. We define e_f as:

$$e_f = \frac{A_{\text{guessed}} + A_{\text{true}}}{A_{\text{true}}}, \tag{84}$$

when the estimated shape does not overlap with the true shape (Fig. 5(a)), and as:

$$e_f = \frac{A_{\text{shaded}}}{A_{\text{true}}}, \tag{85}$$

when the estimated shape partially overlaps with the true shape (Fig. 5(b)):

5.1. *Circular scatterer (acoustic case)*

We discuss first a simple problem in acoustic scattering based on *a priori* information that the target shape is circular, and, consequently, the unknowns are the scatterer's center coordinates and its radius. The shape parameter function $\mathbf{\Psi}$ for such a circular scatterer is defined as:

$$\mathbf{\Psi}(\mathbf{p}) = \begin{Bmatrix} x_0 + R\cos\theta \\ y_0 + R\sin\theta \end{Bmatrix}, \tag{86}$$

where θ ranges from 0 to 2π; $\mathbf{p} = [x_0, y_0, R]$ denotes the vector of the unknown shape parameters, with x_0 and y_0 the cartesian coordinates of the scatterer's center, and R its radius. We use a plane wave with a single incident angle $\alpha = 45°$, and a single probing frequency of $k = 0.1$. The true (target) scatterer is centered at $(3, -10)$ and has a unit

radius, i.e. $\mathbf{p}_{\text{target}} = [3, -10, 1]$. The inversion is initiated with a circular scatterer with radius 1.5, situated at $(-5, -5)$, that is, $\mathbf{p}_0 = [-5, -5, 1.5]$. The response is sampled at three stations located at $(-7, 0)$, $(0, 0)$, and $(7, 0)$ on the free surface; Fig. 6 depicts the problem configuration. Figure 7 shows the convergence path, from the initial guess to the final estimate using the algorithms described herein. We obtained the final estimates as $\mathbf{p}_{\text{final}} = [2.977, -9.986, 0.999]$: they are quite close to the target values. In addition, the convergence pattern of the fitness metric e_f is shown in Fig. 8: at the last iteration the fitness metric is approximately equal to 0.5%.

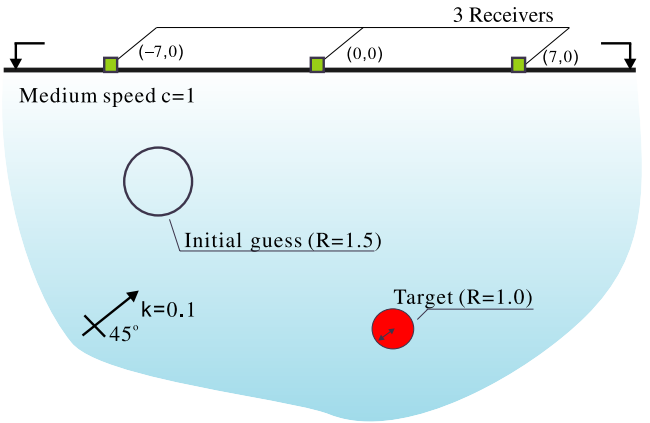

Fig. 6. Problem configuration; circular scatterer (acoustic case).

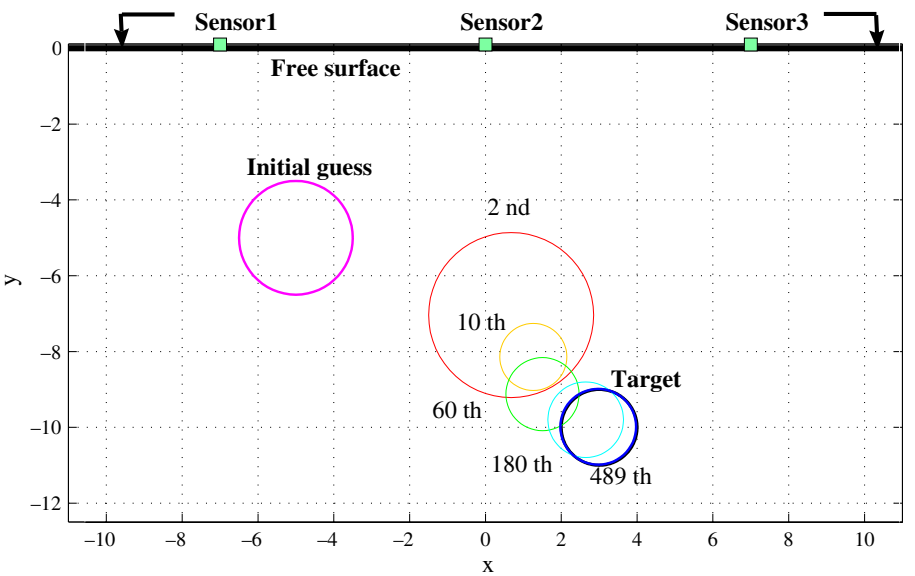

Fig. 7. Convergence path; circular scatterer (acoustic case).

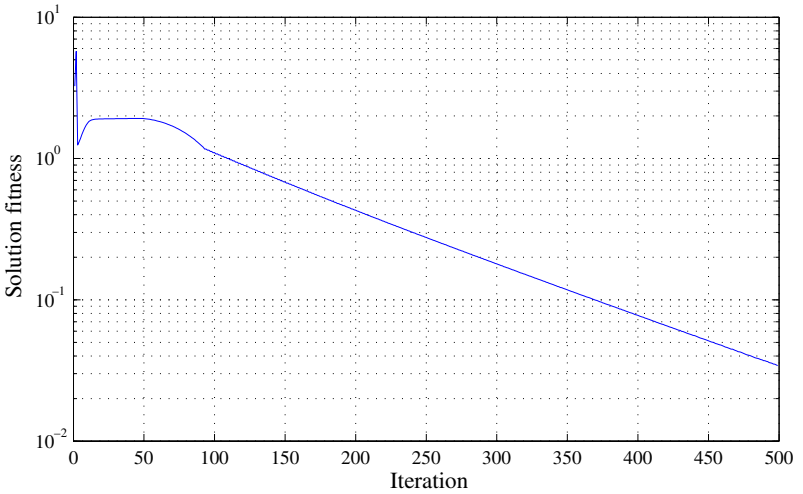

Fig. 8. Solution-fitness; circular scatterer (acoustic case).

5.2. *Elliptical scatterer (SH case)*

For the SH case, we consider an elliptically shaped scatterer with a 4 to 1 ratio of major to minor semi-axes. Accordingly, the unknowns are the scatterer's center coordinates and its semi-axes. The shape parameter function $\boldsymbol{\Psi}$ is thus defined as:

$$\boldsymbol{\Psi}(\mathbf{p}) = \begin{Bmatrix} x_0 + a\cos\theta \\ y_0 + b\sin\theta \end{Bmatrix}, \tag{87}$$

where θ ranges from 0 to 2π, and $\mathbf{p} = [x_0, y_0, a, b]$; (x_0, y_0) are the center coordinates of the ellipse; a, b are the major and minor semi-axes, respectively. The target values are $\mathbf{p}_{\text{target}} = [3.0, -3.0, 2.0, 0.5]$. Our initial guess is a circular scatterer of unit radius with $\mathbf{p}_0 = [-5, -10, 1, 1]$. We use probing waves at a single incidence angle of $\alpha = 45°$, and the surficial responses are sampled at three stations situated at $(-7, 0)$, $(0, 0)$, and $(7, 0)$. We use the frequency continuation scheme with probing frequencies set at $k = 0.1$, 0.5, and 1.0. The problem configuration is shown in Fig. 9, and the convergence path is depicted in Fig. 10. In addition, the estimated parameters are summarized in Table 1, and the convergence pattern of the solution-fitness is depicted in Fig. 11.

As it can be seen in Fig. 10 and Table 1, probing at a low frequency is sufficient to move the estimate close to the target location; when the two higher frequencies of the continuation scheme are used, both the shape and location are fine-tuned (the final fitness metric is 1.7%).

5.3. *Potato-shaped scatterer (acoustic case)*

Next, we consider a potato-(or kidney-)shaped scatterer whose boundary comprises both a concave and a convex part. In this case, we assume that the scatterer is embedded in a

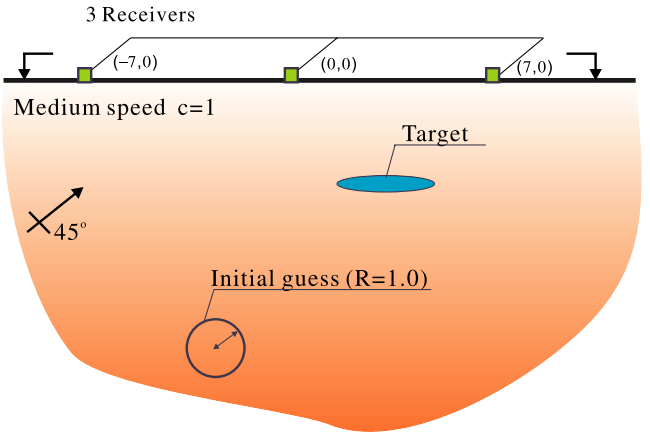

Fig. 9. Problem configuration; elliptical scatterer (SH case).

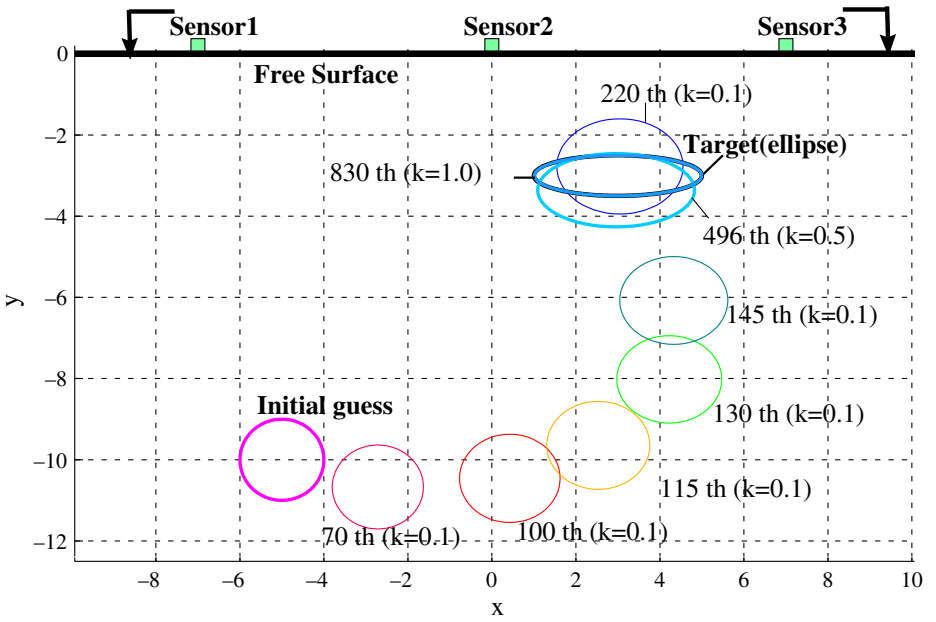

Fig. 10. Convergence path; elliptical scatterer (SH case).

acoustic host medium and the boundary is parameterized as:

$$\boldsymbol{\Psi}(\mathbf{p}) = \left\{ \begin{array}{l} a_1 + \left[a_3 + \displaystyle\sum_{i=1}^{3} \{ a_{2i+2} \cos(i\theta) + a_{2i+3} \sin(i\theta) \} \right] \cos(\theta) \\ a_2 + \left[a_3 + \displaystyle\sum_{i=1}^{3} \{ a_{2i+2} \cos(i\theta) + a_{2i+3} \sin(i\theta) \} \right] \sin(\theta) \end{array} \right\}, \tag{88}$$

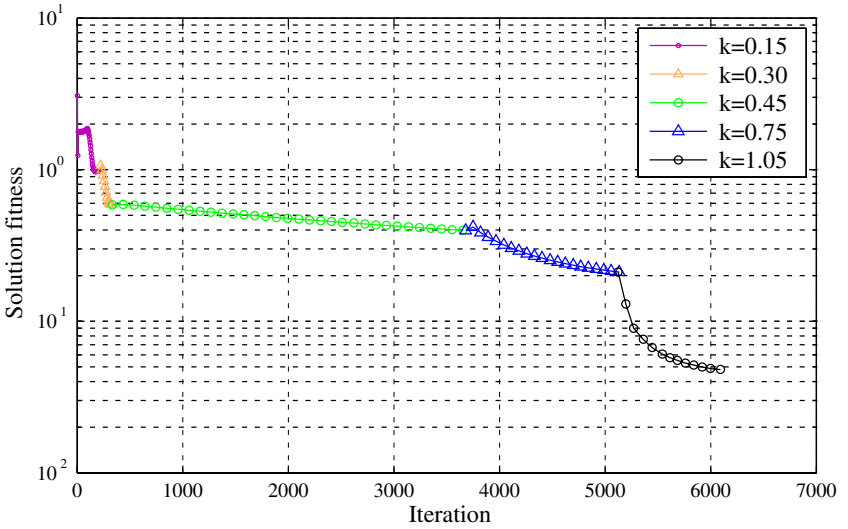

Fig. 11. Solution-fitness e_f; elliptical scatterer (SH case).

Table 1. Final estimated parameters for all probing frequencies; elliptical scatterer (SH case).

Iteration	x_0	y_0	a	b	e_f
initial	3.000	−10.000	1.000	1.000	2.000
220th ($k = 0.1$)	3.047	−2.775	1.503	1.172	1.097
496th ($k = 0.5$)	2.957	−3.361	1.867	0.904	0.905
830th ($k = 1.0$)	3.000	−3.004	−1.978	0.498	0.017
Target	3.000	−3.000	2.000	0.500	—

where θ ranges from 0 to 2π and $\mathbf{p} = [a_1, \ldots, a_9]$. The target parameter vector is $\mathbf{p}_{\text{target}} = [2.0, -10.0, 1.0, 0.2, -0.3, 0.125, 0.125, -0.05, -0.05]$. We initiate the search with a circular scatterer described by the parameter vector $\mathbf{p}_0 = [5, -5, 1.5, 0, 0, 0, 0, 0, 0]$. We use incident waves at two angles of 45° and 135°, respectively, and sample the response at 15 receivers located on the surface between $(-35, 0)$ and $(35, 0)$ at a spacing of 5.0 length units. The problem configuration is depicted in Fig. 12. At the first stage of the inversion process, we set the probing frequency at $k = 0.15$. In addition, we force the assumed shape to remain circular during the first probing frequency in order to prevent the shape from changing in nonphysical ways (e.g. self-intersection), while allowing the assumed shape to approach the vicinity of the true scatterer (Fig. 13). After the target location is roughly recovered during the initial probing, we use four more frequencies set at $k = 0.30, 0.45, 0.75, 1.05$ while simultaneously lifting the shape-constraints. In Fig. 14, the final estimates at every probing frequency are shown and the convergence pattern of the solution-fitness is depicted in Fig. 15. As shown in Fig. 14(b), the finally converged estimates are quite close to the target ($\mathbf{p}_{\text{final}} = [1.88, -10.31, 1.03, 0.28, 0.01, 0.23, 0.14, -0.013, 0.034, 0]$), whereas the final solution-fitness is 4.7%.

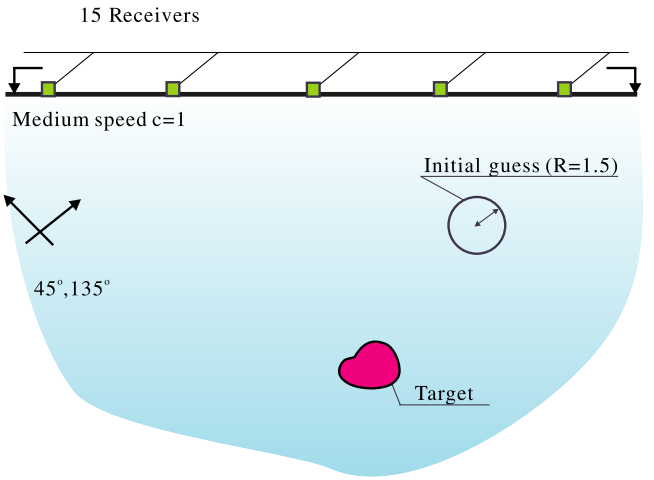

Fig. 12. Problem configuration; potato-shaped scatterer (acoustic case).

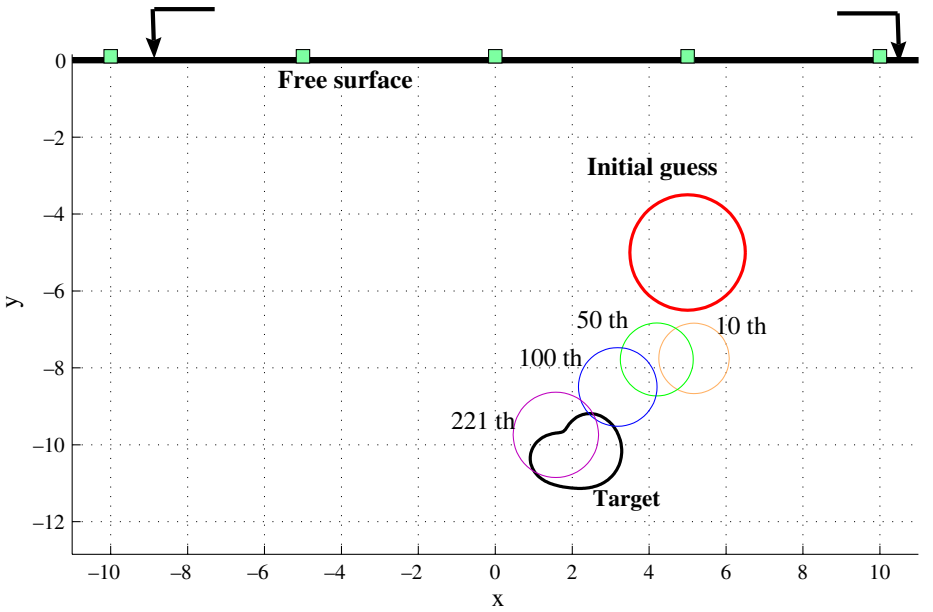

Fig. 13. Convergence path with probing frequency at $k = 0.15$ and circular shape-constraints; potato-shaped scatterer (acoustic case).

5.4. *Kite-shaped scatterer: SH case*

Lastly, we consider a kite-shaped scatterer whose boundary also comprises both convex and concave parts, exposed to SH illumination. The target's shape is defined as:

$$x(\theta) = \cos\theta + 0.65(\cos 2\theta - 1), \tag{89}$$

$$y(\theta) = 1.5\sin\theta - 10, \tag{90}$$

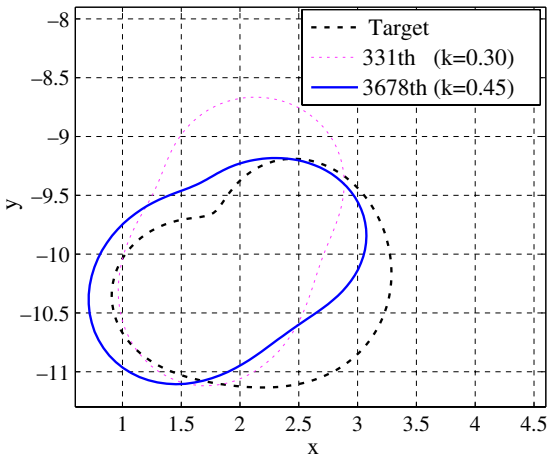

(a) $k = 0.30$ and 0.45

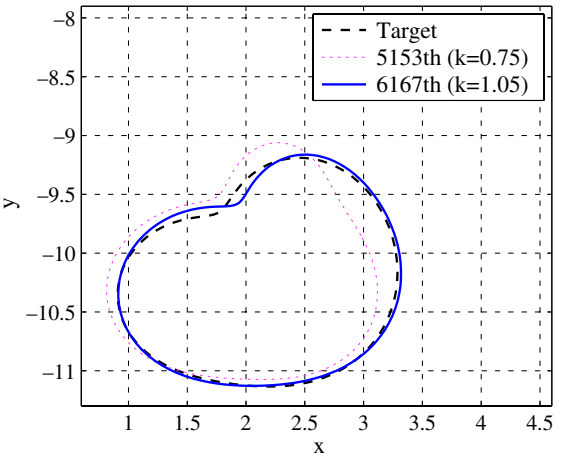

(b) $k = 0.75$ and 1.05

Fig. 14. Final estimates at $k = 0.30, 0.45, 0.75, 1.05$; potato-shaped scatterer (acoustic case).

where θ ranges from 0 to 2π. To approximate the kite's shape, the following boundary parameterization function is used:

$$\boldsymbol{\Psi}(\mathbf{p}) = \begin{Bmatrix} a_1 + \left[a_3 + \sum_{i=1}^{8} \{ a_{2i+2} \cos(i\theta) + a_{2i+3} \sin(i\theta) \} \right] \cos(\theta) \\ a_2 + \left[a_3 + \sum_{i=1}^{8} \{ a_{2i+2} \cos(i\theta) + a_{2i+3} \sin(i\theta) \} \right] \sin(\theta) \end{Bmatrix}, \tag{91}$$

where again θ ranges from 0 to 2π and $\mathbf{p} = [a_1, \ldots, a_{19}]$. We use two incident waves at angles of 45° and 135°, respectively, and measure the surficial response at 15 stations evenly spaced

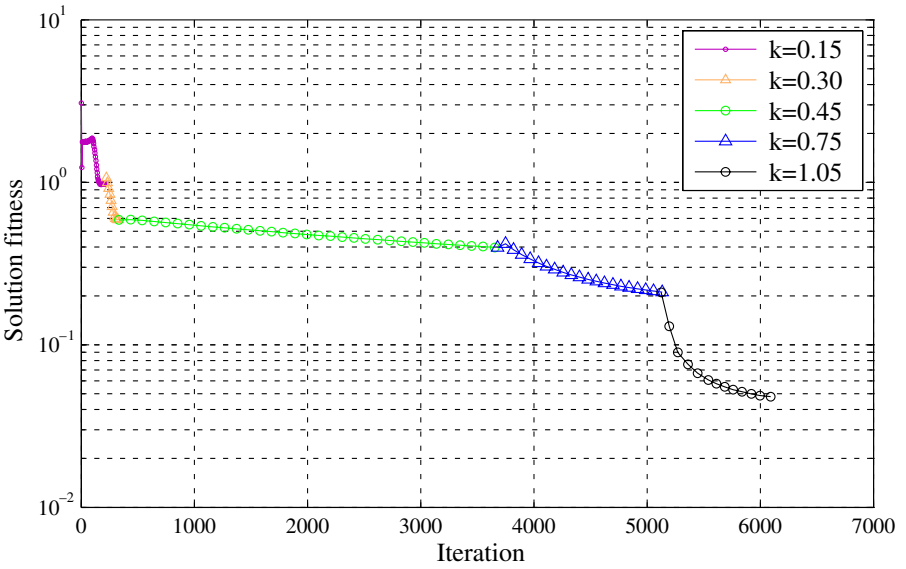

Fig. 15. Solution-fitness; potato-shaped scatterer (acoustic case).

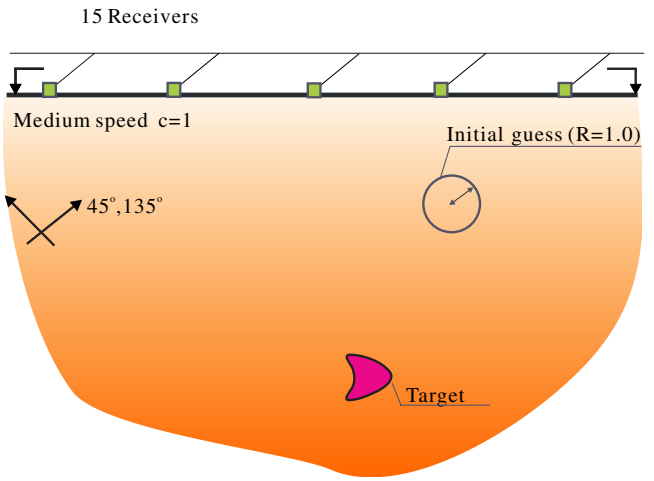

Fig. 16. Problem configuration; kite-shaped scatterer (SH case).

from $(-35, 0)$ to $(35, 0)$ with an interval of 5.0 length units. The problem configuration is presented in Fig. 16.

We start the initial probing with a frequency of $k = 0.1$ and a circular shape; the corresponding parameter vector becomes $\mathbf{p}_0 = [6, -4, 1, 0, \ldots, 0]$. Again, we constrain the initial shape to a circular one until the target location is approximately found (i.e. we have convergence of the method, while enforcing a circular shape). As depicted in Fig. 17, this initial inversion process places the estimate in the vicinity of the target. Then, the shape-constraint is released and the frequency continuation scheme is used over frequencies ranging

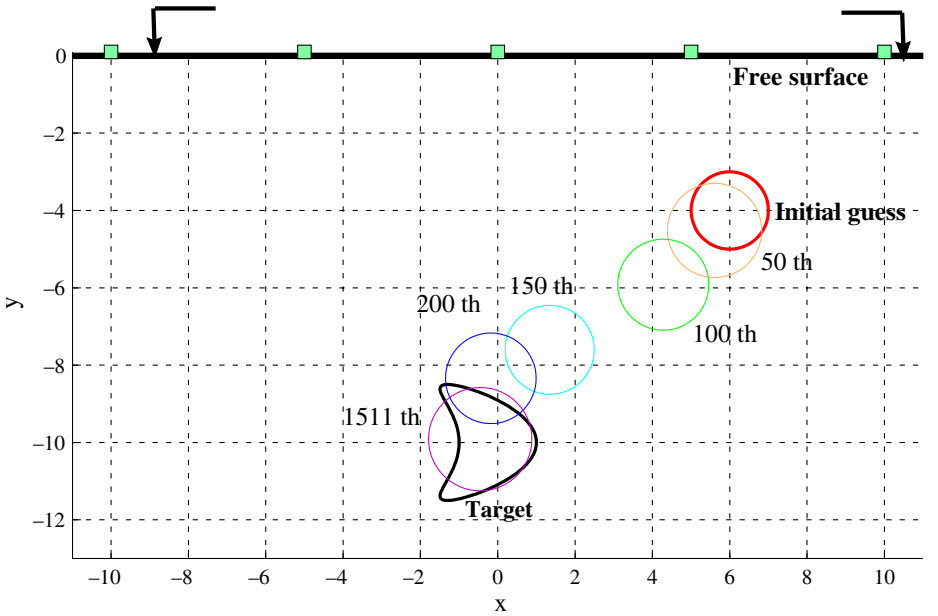

Fig. 17. Convergence path with probing frequency at $k = 0.1$ and circular shape-constraints; kite-shaped scatterer (SH case).

from $k = 0.5$ to 2.1. We obtain a converged shape quite close to the target, as shown in Fig. 18. The associated solution-fitness is approximately 12%, and the final parameter vector is $\mathbf{p}_{\text{final}} = [-0.378, -9.952, 1.210, 0.116, -0.0127, -0.169, -0.0362, 0.310, 0.0390, -0.0934, 0.0160, -0.0444, -0.0241, 0.109, -0.00583, -0.0702, -0.00641, -0.0357, -0.00896]$. While the agreement is not perfect, it is deemed quite satisfactory: we remark further that the solution can be improved by using additional interrogating waves, especially in the case of nonconvex shapes (Fig. 19).

6. Conclusions

We discussed the inverse scattering problem of detecting the shape and location of a scatterer fully immersed in a halfplane, when exposed to illumination by propagating plane waves. In particular, we focused on the two very closely related frequency-domain cases of acoustic and SH waves. We discussed a PDE-constrained optimization approach, endowed with boundary integral equations, for treating systematically the detection problem. For each of the two scalar wave cases, we derived the corresponding state, adjoint, and control problems that, in turn, ensure the satisfaction of the first-order optimality conditions.

Though no direct regularization approach was used, to tackle the multiple minima problem, we employed a three-prong strategy, based on the choice of an amplitude-based misfit functional, a frequency- and/or directionality-continuation scheme, and an *ad hoc* shape-constraining scheme that forces localization at low probing frequencies, prior to shape refinement. We have observed robustness in the recovery of shape and location in

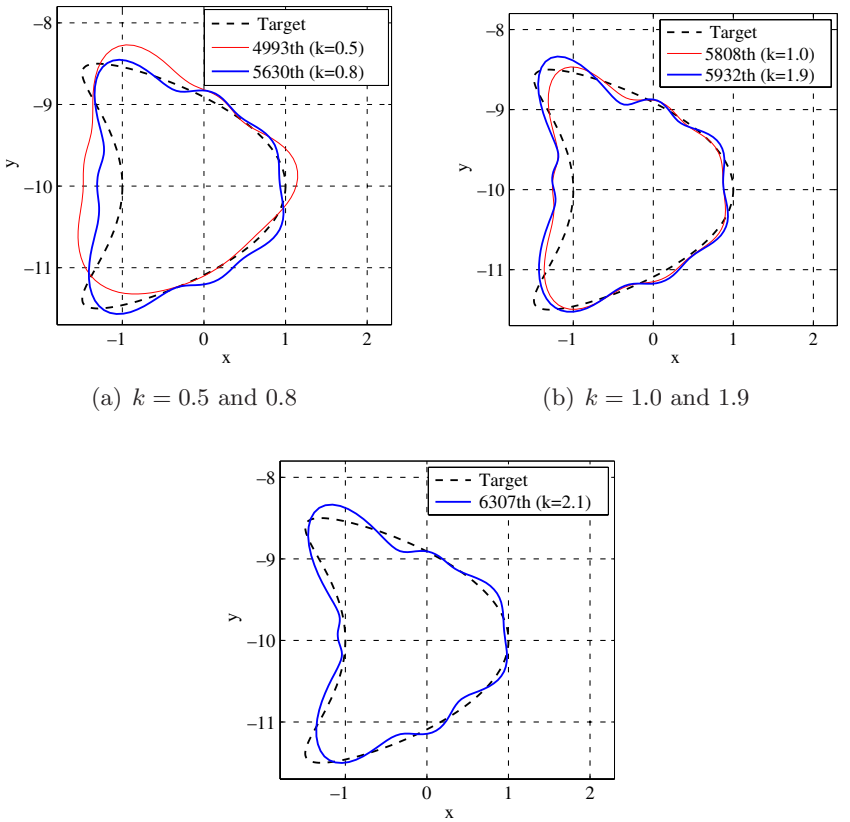

(a) $k = 0.5$ and 0.8

(b) $k = 1.0$ and 1.9

(c) $k = 2.1$

Fig. 18. Final estimates at $k = 0.5, 0.8, 1.0, 1.9, 2.1$; kite-shaped scatterer (SH case).

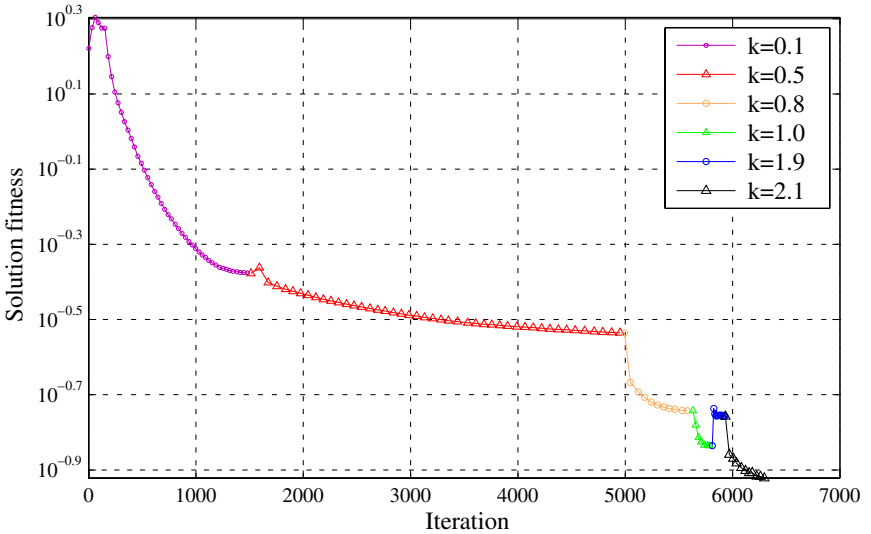

Fig. 19. Solution-fitness; kite-shaped scatterer (SH case).

the reported numerical experiments. Our key observations suggest that low probing frequencies recover the location, whereas higher probing frequencies finetune the shape. The process is, of course, aided, whenever enriched by either additional receivers, or probing waves/incidences, or both.

Acknowledgments

Partial support for the authors' research presented herein has been provided by the National Science Foundation under grant awards CMS-0348484 and ATM-0325125. This support is gratefully acknowledged.

References

1. S.-W. Na and L. F. Kallivokas, PDE-constrained amplitude-based shape detection in inverse acoustic scattering, *Comput. Mech.* **41**(4) (2008) 579–594.
2. B. Guzina, S. N. Fata and M. Bonnet, On the stress-wave imaging of cavities in a semi-infinite solid, *Int. J. Solids Struct.* **40** (2003) 1505–1523.
3. M. Bonnet, BIE and material differentiation applied to the formulation of obstacle inverse problems, *Eng. Anal. Bound. Elem.* **15** (1995) 121–136.
4. D. Colton and R. Kress, *Inverse Acoustic and Electromagnetic Scattering Theory*, 2nd edn. (Springer-Verlag, 1998).
5. D. Colton, J. Coyle and P. Monk, Recent developments in inverse acoustic scattering theory, *SIAM Rev.* **42** (2000) 369–414.
6. A. Kirsch, *An Introduction to the Mathematical Theory of Inverse Problems* (Springer-Verlag, 1996).
7. D. Colton and P. Monk, The inverse scattering problem for time harmonic acoustic waves in an inhomogeneous medium, *Quart. J. Mech. Appl. Math.* **41** (1998) 97–125.
8. A. Kirsch, Factorization of the far-field operator for the inhomogeneous medium case and an application in inverse scattering theory, *Inverse Probl.* **15** (1999) 413–429.
9. D. Colton and A. Kirsch, A simple method for solving inverse scattering problems in the resonance region, *Inverse Probl.* **12** (1996) 383–393.
10. B. Guzina and M. Bonnet, Topological derivative for the inverse scattering of elastic waves, *Quart. J. Mech. Appl. Math.* **57** (2004) 161–179.
11. B. Guzina and Chikichev, From imaging to material identification: A generalized concept of topological sensitivity, *J. Mech. Phys. Solids* **55** (2006) 245–279.
12. B. Guzina and M. Bonnet, Small-inclusion asymptotic of misfit functionals for inverse problems in acoustics, *Inverse Probl.* **22** (2006) 1761–1785.
13. J.-L. Lions, *Optimal Control of Systems Governed by Partial Differential Equations* (Springer Verlag, Berlin, Heidelberg, New York, 1971).
14. H. Petryk and Z. Mróz, Time derivatives of integrals and functionals defined on varying volume and surface domains, *Arch. Mech.* **38** (1986) 697–724.
15. W. Karush, Minima of functions of several variables with inequalities as side constraints, Master thesis, University of Chicago (1939).
16. H. W. Kuhn and A. W. Tucker, Nonlinear programming, ed. J. Neyman, *Proc. the Second Berkeley Symposium on mathematical Statistics and Probability* (Berkeley, CA, USA, 1950).
17. S.-W. Na and L. F. Kallivokas, Continuation schemes for shape detection in inverse acoustic scattering problems, *Computer Modeling in Engineering & Sciences* **35** (2008) 73–90.